Atmos. Chem. Phys. Discuss., doi:10.5194/acp-2016-171, 2016
Manuscript under review for journal Atmos. Chem. Phys.
Published: 13 April 2016

Atmospheric Chemistry and Physics Discussions

Vertical profiles of aerosol and black carbon in the Arctic: a seasonal phenomenology along two years (2011-2012) of field campaign

Luca Ferrero[1], David Cappelletti[2,3], Maurizio Busetto[3], Mauro Mazzola[3], Angelo Lupi[3], Christian Lanconelli[4], Silvia Becagli[5], Rita Traversi[5], Laura Caiazzo[5], Fabio Giardi[5], Beatrice Moroni[2], Stefano Crocchianti[2], Martin Fierz[6], Grisa Mocnik[7,8], Giorgia Sangiorgi[1], Maria G. Perrone[1], Marion Maturilli[9] and Vito Vitale[3], Roberto Udisti[5], Ezio Bolzacchini[1]

[1]Department of Earth and Environmental Sciences, University of Milano-Bicocca, Piazza della Scienza 1, 20126, Milano, Italy

[2]Department of Chemistry, Biology and Biotechnology, University of Perugia, 06123 Perugia, Italy.

[3]ISAC CNR, Via Gobetti 101, 40129, Bologna, Italy

[4]European Commission, Joint Research Centre (JRC), Institute for Environment & Sustainability, via E. Fermi, 2749 - 21027 Ispra (VA), Italy

[5]University of Florence, Via della Lastruccia 3, 50019, Sesto Fiorentino, Florence Italy

[6]University of Applied Sciences Northwestern, Switzerland, Windisch, Switzerland

[7]Aerosol d.o.o., Kamniska 41, SI-1000 Ljubljana, Slovenia

[8]Condensed Matter Physics Department, Jozef Stefan Institute, Jamova 39, SI-1000 Ljubljana, Slovenia

[9]Alfred Wegener Institute, Helmholtz Centre for Polar and Marine Research, Telegraphenberg 43A, 14473 Potsdam, Germany.

Correspondence to: Luca Ferrero (luca.ferrero@unimib.it)

Abstract. In this paper we present results from a systematic study of vertical profiles of aerosol number size distribution and black carbon (BC) concentrations conducted in the Arctic, over Ny-Ålesund (Svalbard). The campaign lasted 2 years (2011-2012) and resulted in 200 vertical profiles measured during the spring and summer seasons. In addition, chemical analysis of filter samples, aerosol size distribution and a full set of meteorological parameters were determined at ground to put on a firmer grounds the analysis of the vertical profiles. The collected experimental data allowed a classification of the vertical profiles into different typologies which allowed to describe a seasonal phenomenology of vertical aerosol properties in the Arctic.

During spring, four main types of profiles were found and their behaviour was related to the main aerosol and atmospheric dynamics occurring at the measuring site. Background conditions generated homogenous profiles. Transport events caused an increase of aerosol concentration with altitude. High Arctic haze pollution trapped below thermal inversions promoted a decrease of aerosol concentration with altitude. Finally, ground-based plumes of locally formed secondary aerosol determined profiles with decreasing aerosol concentration located at different altitude in function of size.

Atmos. Chem. Phys. Discuss., doi:10.5194/acp-2016-171, 2016
Manuscript under review for journal Atmos. Chem. Phys.
Published: 13 April 2016

Atmospheric Chemistry and Physics Discussions

During the summer season, the impact from shipping caused aerosol and BC pollution plumes constrained close to the ground, indicating that increasing shipping emissions in the Arctic could bring anthropogenic aerosol and BC in the summer Arctic affecting the climate.

1 Introduction

The Arctic is subject to an amplification of the global warming as the observed temperature increase has been almost twice than the global average (IPCC, 2013; Serreze and Barry, 2011; Shindell and Faluvegi, 2009) giving as a consequence the first complete opening of the Northwest Passage in 2007 (Serreze et al., 2007) together with a greening of the coastal tundra (Bhatt et al., 2010) and altered wind patterns (Overland and Wang, 2010).

The Arctic amplification is the result of complex global feedbacks (acting at different spatial and temporal scales) involving the impact of sea ice changes on the heat fluxes between the ocean and the atmosphere (Screen and Simmonds, 2010a and 2010b), the effect of changes in the cloud cover and water vapour on the longwave radiation fluxes (Francis and Hunter, 2006), the changes in atmospheric and oceanic heat transports (Yang et al., 2010), the black carbon (BC) deposition on the snow (Hansen and Nazarenko, 2004) and the changes in the atmospheric BC and aerosol concentrations themselves (Flanner, 2013; Serreze and Barry, 2011; Shindell and Faluvegi, 2009).

Many of these feedbacks can be altered by the aerosol due to its ability to absorb and scatter the solar radiation (direct effect), to seed and modify the cloud properties (indirect effects) and to influence with semi-direct effects the atmospheric properties (i.e. the thermal structure) (IPCC, 2013; Ramanathan and Feng, 2009; Koren et al. 2008; Koren et al., 2004; Kaufman et al., 2002). With respect to the role of aerosol, Shindell and Faluvegi (2009) estimated that globally the decreasing concentrations of sulphate aerosols and the increasing concentrations of BC contributed (during 1976–2007) with 1.09±0.81 °C to the Arctic surface temperature increase of 1.48±0.28 °C.

As tropospheric aerosol particles are Short-Lived Pollutants (~one-few weeks of residence time) and act as Short-Lived Climate Forcers their effect could be controlled by short-term climate strategies (Ødemark et al., 2012; Shindell et al., 2012; Jacobson, 2010; Quinn et al., 2008) opening up an opportunity for policymakers. However, to adopt the right mitigation strategies, it is necessary to distinguish the Arctic warming effect caused by advection and by local emitted aerosol (Flanner, 2013; Sand et al., 2013; Shindell and Faluvegi, 2009)

Focusing on the Arctic aerosol, a crucial question is: how the vertical distribution of the aerosol properties seasonally varies?

The importance of this question comes from two observations.

First of all, the aerosol properties (size distribution, chemical composition, optical properties) in the Arctic exhibit a very pronounced seasonal variation; this is due to an interplay of changes in the dominating sources (outside or inside the Arctic region) with meteorological conditions that allow or inhibit the transport from source regions (Quinn et al., 2008; Eckhardt et al., 2003). The spring period is characterized by the presence of the Arctic Haze dominated by the accumulation mode aerosol (enriched in BC); the summer period is dominated by the small Aitken particles which are locally formed (with a negligible BC content) (Tunved et al., 2013; Spackman et al., 2010;Eleftheriadis et al., 2009; Ström et al., 2003 and 2009; Udisti et al., 2013; Viola et al., 2013). The second observation is that, the same type of aerosol can produce different climatic effects (warming or cooling) depending on its location within the atmospheric column and may trigger different kinds of local feedbacks (snow/ice-albedo, clouds) (Flanner, 2013; Sand et al., 2013; Shindell and Faluvegi, 2009).

Atmos. Chem. Phys. Discuss., doi:10.5194/acp-2016-171, 2016
Manuscript under review for journal Atmos. Chem. Phys.
Published: 13 April 2016

Atmospheric Chemistry and Physics Discussions

For example, it is well know that BC aerosol absorbs solar radiation and heats the surrounding air (Ferrero et al., 2014 and 2011; Samset et al., 2014; Samset et al., 2013; Ramana et al., 2007). However, it has been demonstrated that the surface temperature response varies considerably with the altitude of the induced heating: BC may potentially warm the Arctic, if the BC is located immediately above snow and ice while, if BC is located in the Arctic free troposphere leads to an opposite result reducing the surface air temperature and promoting the increase in the sea-ice fraction despite the positive BC forcing at the top of the atmosphere (Flanner, 2013; Brock et al., 2011; Seinfeld and Pandis, 2006; Hansen and Nazarenko, 2004). This phenomenon is due to a combination of the weakening of the northward heat transport, caused by a reduction in the meridional temperature gradient, and the increasing of atmospheric stability caused by the contemporary dimming of the surface and heating aloft, resulting in a reduction of the downward sensible heat flux(Flanner, 2013; Sand et al., 2013; Shindell and Faluvegi, 2009).

Not only the BC vertical distribution is crucial, but also that of the total aerosol particles, which can influence the indirect effect and the related feedbacks. Changes in the cloud cover (especially low-level Arctic stratus) increases the downward longwave flux to the surface in function of the cloud base temperature and cloud phase (liquid, mixed or ice) (Serreze and Barry, 2011; Francis and Hunter, 2006). As reported in literature, low clouds mainly warm the surface in the Arctic (with the exception of a brief period in summer) (Vavrus et al., 2009; Intrieri et al., 2002) due to the stable stratified conditions that often prevail in the Arctic (Manabe and Wetherald, 1975). Because the highest number density of aerosol particles observed in the Arctic is due to a locally formed aerosol (mainly in summer as stated above) (Tunved et al., 2013; Engvall et al., 2008; Ström et al., 2003) it is important to assess the vertical behaviour of the aerosol concentration in function of its size and the season.

However, up till now, aerosol vertical profiles in the Arctic are scarse compared with the number of available data collected at ground level (Samset et al., 2013; Koch et al., 2009); more vertical measurements are being carried out only recently. The available measurements were conducted mainly using aircraft and thus were mainly limited to short-time campaigns (Kupiszewski et al., 2013;Bates et al., 2013; Spackman et al., 2010;Schwarz et al., 2010;Koch et al., 2009). Spackman et al.(2010) and Koch et al. (2009) reported BC located mainly in the Arctic free troposphere while Schwarz et al. (2010) found highest BC concentration close to the ground. These reports may well highlight opposing forms of behaviour of vertical aerosol properties both for the aerosol's size distribution and for the aerosol's chemical composition along height.

In addition to this, aerosol vertical distribution could be affected in the future by changes in the aerosol emissions within the Arctic itself: the increasing of shipping emission in the Arctic is a good example. Shipping emissions should inject the BC directly into the Arctic planetary boundary layer (warming the surface and depositing on snow and ice). The importance of the increasing shipping emission in the Arctic has been recently underlined (Eckhardt et al., 2013; Corbett et al., 2010; Granier et al., 2006). Although the final impact is debated (Browse et al., 2013), the effective vertical distribution of these emissions has not yet been investigated.

Thus, there is a clear need to also improve the knowledge about aerosol vertical profiles in the Arctic during week-long campaigns along years to find common rules of behaviour.

With respect to this, the Arctic site of Ny-Ålesund (Svalbard Islands) is particularly suitable, featuring long term data series of ground based aerosol properties, lidar profiles, radiometric and meteorological data (Maturilli et al. 2015; Tunved et al., 2013; Di Liberto et al., 2012; Vihma et al., 2011; Hoffmann et al., 2009;Eleftheriadis et al., 2009; Eleftheriadis et al., 2004; Stock et al., 2012; Ström et al., 2003, 2009).

Atmos. Chem. Phys. Discuss., doi:10.5194/acp-2016-171, 2016
Manuscript under review for journal Atmos. Chem. Phys.
Published: 13 April 2016

Atmospheric Chemistry and Physics Discussions

Despite this substantial amount of data, aerosol and BC measurements along vertical profiles over Ny-Ålesund are, up to now, reported to be sparse (Bates et al., 2013; Lawson et al., 2011; Engvall et al., 2008).

This paper tries to fill this gap reporting aerosol and BC vertical profiles measured over Ny-Ålesund (Svalbard Islands) along two years (2011-2012) during an extensive field campaign that allowed collecting data for more than 200 vertical profiles. Vertical profiles measurements were conducted in the framework of the PRIN2009 "ARCTICA" project. The main part of the scientific activities at Ny-Ålesund was aimed at studying the chemical and physical properties of the aerosols and the long-range transport processes of organic and inorganic species at the site and along vertical profiles (Moroni et al., 2015; Udisti et al., 2013).

In the next sections we briefly describe the sampling sites (section 2.1) and the vertical profile measurements (section 2.2). Results and discussion follow in section 3, with the conclusions in the final section 4.

2 Methodology

Tethered balloon soundings were carried out during spring 2011 and summers 2011and 2012 over Ny-Ålesund, a research community that is located at the Kongsfjorden, a fjord that develops in the north-west south-east direction. Northwards, Ny-Ålesund faces the sea, while a small chain of 400-500 m high mountains is located to the South (Figure1a).

Vertical profiles were measured from two sampling sites: the Italian CNR Gruvebadet sampling site(78°55'03"N 11°53'40"E; Figure 1b) in spring and from the German-French AWIPEV research base (78°55'24" N 11°55'15"E) in summer. The locations were chosen to increase the distance from the Ny-Ålesund village in Spring and to lie in the proximity of the Ny-Ålesund harbour in Summer (to highlight the ship plume diffusion over Ny-Ålesund; section 3.3). Table 1 resume the dates of the campaign, the number of flights, the maximum altitudes and the cloud base height (when present).

The aerosol and meteorological measurements were carried out both at ground and along the profiles; they are here below described starting from ground-based measurements (section 2.1), followed by that collected along vertical profiles (section 2.2).

2.1 Ground-based measurements

Ground-based measurements were carried out at the Gruvebadet laboratory (Figure 1b), whose geographical position (1 km southern Ny-Ålesund) guarantees for the lowest impact form local emissions. A clean area was established in the north-east side overlooking the Ny-Ålesund village and snow mobile traffic and other potentially contaminant activities were forbidden.

The Gruvebadet laboratory is equipped with a series of instruments aimed at measuring physical, optical properties of aerosol and to collect aerosol samples for chemical analysis (section 2.1.1).

The aerosol size distribution was measured using a Scanning Mobility Particle Sizer (TSI-SMPS 3034, 54 size classes, 10–487 nm) coupled with an Aerodynamic Particle Sizer (TSI-APS 3321, 52 classes, 0.5– 20 μm). The two coupled systems measure one size spectrum every 10 minutes.

PM samples are collected through both high-volume and low volume samplers. For the purpose of the present paper, PM_{10} samples collected using two TECORA SkyPost low-volume sampler (EN 12341; PM_{10} sampling head, flow 2.3 m^3 h^{-1}; PTFE and and quartz microfiber filters, Ø=47 mm) were considered. Samplings were carried out in actual conditions: pressure and temperature were continuously monitored in order to maintain the constant flow

Atmos. Chem. Phys. Discuss., doi:10.5194/acp-2016-171, 2016
Manuscript under review for journal Atmos. Chem. Phys.
Published: 13 April 2016

Atmospheric Chemistry and Physics Discussions

rate of 2.3 m^3 h^{-1}. The first sampler collected PM_{10} for 24 h on Teflon filters (Pall R2PJ047) to determine the ionic fraction while the second one collected PM_{10} for 96 h on pre-fired Quartz microfiber filters (chm QF1 grade) to determine the Elemental and Organic Carbon (section 2.1.1). The filters were conditioned for 48 hours (25°C and 50% relative humidity) before and after the sampling, then weighted by a 5-digit microbalance (Sartorius ME235P). Uncertainties on mass concentrations are lower than 5%.

After sampling, filters were individually sealed in pre-washed (with Milli-Q water, 18.3 MΩ cm) polystyrene filter containers and stored at – 20°C until analysis.

2.1.1 Aerosol chemistry measurements at ground level

PM_{10} samples collected at ground-level at Gruvebadet were analysed to determine first the water-soluble ionic fraction. Half of each PM_{10} Teflon filter was extracted in 10 ml of ultrapure water (Milli-Q, 18.3 MΩ cm) by ultrasonic bath for 20 min. Filter manipulation was carried out under a class-100 laminar-flow hood, in order to minimize contamination risks.

Inorganic cations and anions together with organic anions, were simultaneously measured by a triple Dionex ion-chromatography system, equipped with electrochemical-suppressed conductivity detectors.

More in detail, cations (Na^+, NH_4^+, K^+, Mg^{2+} and Ca^{2+}) have been determined by a Dionex CS12A-4 mm analytical column with 20 mM H_2SO_4 eluent; anions (Cl^-, NO_3^-, SO_4^{2-} and $C_2O_4^{2-}$) were measured by a Dionex AS4A-4 mm analytical column with a 1.8 mM Na_2CO_3 / 1.7 mM $NaHCO_3$ eluent while F^- and some organic anions (acetate, glycolate, formate and methanesulfonate) were determined by a Dionex AS11 separation column by a gradient elution (0.075 mM to 2.5 mM $Na_2B_4O_7$ eluent) (Udisti et al., 2004;Becagli et al., 2011).

As the contribution of sea salt and crustal components in Ny-Ålesund is not-negligible (Udisti et al., 2015; Giardi et al., 2015; Moroni et al., 2015), Na^+, Ca^{2+} and SO_4^{2-}(which originate from both these sources) were apportioned between sea-salt (ss-) and non-sea-salt (nss-) fractions in every sample on the basis of known w/w (weight/weight) ratios in sea water and Earth crust (Udisti et al., 2015; Giardi et al., 2015; Becagli et al., 2012; Udisti et al., 2012) as follows:

$$\text{tot-}Na^+ = \text{ss-}Na^+ + \text{nss-}Na^+ \quad (1)$$

$$\text{tot-}Ca^{2+} = \text{ss-}Ca^{2+} + \text{nss-}Ca^{2+} \quad (2)$$

$$\text{ss-}Na^+ = \text{tot-}Na^+ - 0.562\ \text{nss-}Ca^{2+} \quad (3)$$

$$\text{nss-}Ca^{2+} = \text{tot-}Ca^{2+} - 0.038\ \text{ss-}Na^+ \quad (4)$$

where 0.562 represents the w/w Na^+/Ca^{2+}ratio in the crust (Bowen, 1979) and 0.038 is the Ca^{2+}/Na^+ w/w ratio in seawater (Nozaki, 1997).

Similarly, the ss-SO_4^{2-} fraction was calculated from the ss-Na^+ using the 0.253 SO_4^{2-}/Na^+ w/w ratio in seawater (Bowen, 1979).The crustal fraction of sulfate (cr-SO_4^{2-}) was determined from the nss-Ca^{2+} using the 0.59 SO_4^{2-}/Ca^{2+} w/w ratio in the uppermost Earth crust (Wagenbach et al., 1996). Finally, the nss-nc-SO_4^{2-} fraction, which can be due to anthropogenic or secondary formed aerosol, was calculated by subtracting the ss- $SO_4^{2-}$and cr-SO_4^{2-} contributions from the total SO_4^{2-} concentrations.

In addition to ionic fraction determination, also the Elemental Carbon (EC) and the Organic Carbon (OC) fraction were determined on PM_{10} samples through a Thermo-Optical Transmission (TOT) method following the NIOSH protocol.

Atmos. Chem. Phys. Discuss., doi:10.5194/acp-2016-171, 2016
Manuscript under review for journal Atmos. Chem. Phys.
Published: 13 April 2016

Atmospheric Chemistry and Physics Discussions

The organic matter (OM) was calculated by multiplying the OC fraction by 2.1 (Turpin and Lim, 2001) typical for remote sites characterized by high impact of secondary sources.

2.1.2 Meteorological Context

Meteorological parameters are currently measured at different sites in Ny-Alesund.. Close to the summer campaign balloon launch site, the German-French AWIPEV research base operates surface meteorology measurements with 1-minute time resolution, including temperature and relative humidity at 2 meter height, wind speed and direction at 10 meter height, and pressure at station level (Maturilli et al., 2013). Also the cloud base height in the vertical column above the station is retrieved, using a Vaisala LD-40 ceilometer. Every day at 1100 UTC, a radiosonde is launched to monitor the thermodynamic profile from ground to about 30 km, providing auxiliary profile data for the aerosol profile analysis. As to these long-term observations, the campaign periods spring 2011, summer 2011, and summer 2012 can be put into a climatological context.

The National Research Council of Italy (CNR) operates since 2009 the Amundsen-Nobile Climate Change Tower, that provides meteorological, micro-meteorological, radiation and snow measurements continuously all year-long (Mazzola et al. 2015a). Conventional and micro-meteorological parameters are measured at different heights (4 and 3 levels, respectively) in order to investigate their vertical variations in different situations. By analysing micro-meteorological data, Dai et al. (2011) and Mazzola et al. (2015b) found that both in the Adventfjorden and in Kongsfjorden, where Ny-Ålesund is located, the atmosphere is stable for about 50% of the time along the year. In these cases, the vertical mixing of the aerosols is not encouraged. Looking in details to micro-meteorological data for the periods concerning the campaigns, we found that this percentage is similar for the spring period, while during the summer campaigns atmospheric instability is favoured. This is clearly related to a different heating of the ground during snow covered or not periods.

2.2 Vertical profile measurements

Vertical profile measurements were carried out by means of a kytoon-shape helium-filled tethered balloon (lenght 8 m, Ø=3 m, volume 55.0 m^3, payload 25 kg, Figure 1c. The tethered balloon was designed to fly in severe wind conditions. However, for security reasons, it was mainly used during low wind conditions (wind speeed mainly less than 10 m s^{-1}).

The tethered balloon was equipped with an instrumental package consisting of:

1) an Optical Particle Counter (OPC GRIMM *1.107*; 31 size classes between 0.25 to 32 μm, 6 sec sampling time) for the particle number size distribution determination;

2) a miniaturized electrical particle detector (miniDiSC, Matter Aerosol) to measure the total particle number concentration (1 sec sampling time);

3) two micro-Aethalometers: the microAeth® AE51 and a new prototype (Magee Scientific, 1-60 sec sampling time);

4) a meteorological station (LSI-Lastem: pressure, temperature and relative humidity, 6 sec sampling time).

During the period 11/04/2011-30/04/2011 the Vaisala tethersonde TTS111 (pressure, temperature, relative humidity, wind speed and wind direction; 1 sec sampling time) was used.

Atmos. Chem. Phys. Discuss., doi:10.5194/acp-2016-171, 2016
Manuscript under review for journal Atmos. Chem. Phys.
Published: 13 April 2016

Atmospheric Chemistry and Physics Discussions

The maximum height reached during each flight depended on atmospheric conditions and, for the majority of profiles, was between 0.7 and 1.3 km. An electric winch controlled the ascent/descent rates that were set at 40.0 ± 0.1 m/min.

Among the whole ensemble of collected data by the instrumentation package, mainly size distribution, BC and meteorological data will be presented here for the purpose of the present paper.

Due to the low aerosol concentrations present in the Arctic, a deeper description of the collected data, their accuracy and the data treatment are here below discussed for each instrument (sections 2.2.1 and 2.2.2). Moreover, as the aim of the paper is the determination of the aerosol properties along height, in section 2.2.3 the determination of aerosol stratifications is discussed.

2.2.1 Size distribution data

In this study, the total aerosol concentration and the number size-distribution along height was measured using a coupled miniDiSC –OPC (λ=655 nm) system.

The miniDiSC is a miniature Diffusion Size Classifier, a small and portable instrument (4×9×18 cm, 670 g, 8h of battery supply) based on unipolar charging of the aerosol, followed by detection in two electrometer stages (Fierz et al., 2011). The aerosol is first charged in a standard positive unipolar diffusion charger (the average charge is approximately proportional to the particle diameter), than the charged particles flow through a diffusion stage (an electrically insulated stack of stainless steel screens connected to a sensitive electrometer that collect the finest particles) and into a second stage (equipped with a HEPA filter) where the current of larger particles is measured with an electrometer.

The miniDiSC has a d_{50} cutoff at 14 nm. Thus, the instrument underestimates particle number concentrations (even it is partially calibrated for) for particles smaller than 20 nm (Nucleation Mode). As a result, the miniDiSC counts only partially the Nucleation Mode while, above it, it allows a whole determination of Aitken and Accumulation Mode particles. As demonstrated by Fierz et al. (2011), a bimodal lognormal aerosol size distribution with a fixed accumulation mode at 100 nm and a varying nucleation mode at 20 nm introduce an underestimation of about -2% – -10% of the total aerosol concentration in the miniDiSC response. The particle number determination is robust, and the error never exceeds 20%.

The OPC used in the campaign was the model the Grimm *1.107* that counts and classifies the aerosol in 31 size classes between 250 nm and 32 µm. As reported in literature (Ferrero et al., 2014; Howell et al., 2006; Heyder and Gebhart, 1979), OPCs size classification of the aerosol particles is a function of their ability to scatter the laser light under the assumption of spherical particles. The aerosol particles are classified in terms of their optical equivalent diameter which is defined as “the diameter of a sphere of known refractive index (that of polystyrene latex spheres used for of calibration) that scatters light as efficiently as the real particle in question”. This effect usually results in an “undersizing” of the size classification, due to the higher refractive index of the polystyrene latex spheres (PSL spheres, m=1.58 at 655 nm; Ma et al., 2003) used in the OPC calibration compared to ambient aerosol (Guyon et al., 2003; Liu and Daum, 2008; Schumann, 1990). In order to derive a proper size classification of the aerosol over Svalbard, the “undersizing” issue was solved by correcting the OPC size channels to account for the ambient aerosol refractive index m. The OPC response function (*S:* the partial light scattering cross section

Atmos. Chem. Phys. Discuss., doi:10.5194/acp-2016-171, 2016
Manuscript under review for journal Atmos. Chem. Phys.
Published: 13 April 2016

Atmospheric Chemistry and Physics Discussions

of the particle related to the specific optical design of the OPC) was computed at 655 nm as follows (Baron and Willeke, 2005; Heyder and Gebhart, 1979):

$$S(\theta_0, \Delta\Omega, x, m) = \frac{\lambda^2}{4\pi^2} \iint_{\Delta\Omega} i(\theta, \Phi, x, m) sin\theta d\theta d\Phi \quad (5)$$

where θ_0 represents the mean scattering angle of the optical arrangement, $\Delta\Omega$ the receiver aperture, x the dimensionless size parameter, m the refractive index and $i(\theta,\phi,x,m)$ the Mie scattering function composed by the perpendicular and parallel components $i_1(\theta,x,m)$ and $i_2(\theta,x,m)$ respectively. The optical arrangement of the OPC 1.107 consists of: 1) a wide angle parabolic mirror (121°, from 29.5° to 150.5°, θ_0=90°)that focuses scattered light on the photodetector located on the opposite side; 2) 18° of direct collected scattered light on the photodetector (from 81° to 99°, θ_0=90°) (Heim et al., 2008).

The response function was calculated both for PSL spheres (S_{PSL}) and for ambient aerosol (S_{AMB}). The refractive indexes of ambient aerosol used in S_{AMB} calculations were obtained from the closets AERONET site (Horsund site, 77°00'04" N 15°33'37" E) for spring 2011 and summer 2011-2012: 1.544+0.013i and 1.535+0.015i, respectively. These refractive indexes are referred at 674 nm (the closest AERONET wavelength to the OPC laser wavelength of 655 nm) and were close to those determined at530 nm at Gruvebadet site (range 1.4-1.8 during 2010 and 2011) as reported in the work of Lanconelli et al., (2013).

Table S1 shows the new size corrected channels in comparison with the PSL spheres equivalent ones. The new channels were used to define three broad-size ranges (detailed here below) to evaluate the vertical behaviour of aerosol.

The coupled miniDiSC–OPC (λ=655 nm) system measurement range covers the relevant region of the aerosol number size-distribution. In order to study the behaviour of different size classes along height, three aerosol number concentration size ranges were selected:

1) the number concentration of aerosol between 14 nm (d_{50} of miniDiSC) and 260 nm (cfr Table S1) obtained as the difference between the total number concentration measured by the miniDiSC and that measured by the OPC, hereinafter indicated as $N_{14\text{-}260}$;

2) the number concentration of aerosol between 260 nm (lower limit of OPC) and 1200 nm hereinafter indicated as $N_{260\text{-}1200}$;

3) the number concentration of aerosol above 1200 nm, hereinafter indicated as $N_{>1200}$.

The $N_{14\text{-}260}$ includes a small fraction of the Nucleation mode (from 14 to 20 nm), the totality of the Aitken mode (20-100 nm) and a fraction of the Accumulation mode (from 100to 260 nm); $N_{260\text{-}1200}$ includes most of the Accumulation mode particles and thus, it will be hereinafter also addressed as Accumulation mode particles along the discussion; finally, $N_{>1200}$ covers the totality of Giant Nuclei mode and will be referred to as "coarse fraction".

The accuracy of both miniDiSC and OPC measurements was investigated comparing the lowermost portion of their measurements along vertical profile with SMPS+APS data collected at ground-level at Gruvebadet. This comparison was performed during spring 2011 to avoid any summer deviation related to a different ship plume dispersion starting from Ny-Ålesund harbour towards Gruvebadet (in summer balloon sounding were conducted from the Koldeway station instead that from Gruvebadet; section 2.1). Figure 2a-b shows the results of this comparison for $N_{14\text{-}260}$ (miniDiSC vs. SMPS) and $N_{>260}$ (OPC vs. SMPS+APS) which was characterized by an excellent correlation (R^2>0.9) with linear best fits close to the ideal ones and an average error of 7% and 16% for $N_{14\text{-}260}$ and $N_{>260}$, respectively. These results highlight the reliability of measurements carried out along the vertical

Atmos. Chem. Phys. Discuss., doi:10.5194/acp-2016-171, 2016
Manuscript under review for journal Atmos. Chem. Phys.
Published: 13 April 2016

Atmospheric Chemistry and Physics Discussions

profiles, an important feature considering the low aerosol concentration values and their variation, which are present within the Arctic (section 1).

2.2.2 Black Carbon

BC have been determined using two micro-Aethalometers: the microAeth® AE51 and a new prototype (Magee Scientific; 250 g, 117x66x38 mm^3).

AE51 and the prototype were identical with the exception that the prototype measured at 2-λ (370 and 880 nm) while AE51 only at 880 nm. At the time of campaign the prototype was just yet developed and was used instead the AE51 on the balloon platform during the spring 2011 campaign only when necessary (i.e. AE51 in charge) to ensure the continuity of measurements during the campaign.

In both the Aethalometers the aerosol containing BC was continuously sampled onto a PTFE-coated borosilicate glass fiber filter (Fiberfilm™ Filters, Pall Corporation) where the light attenuation (*ATN*) was measured at 880 nm relative to a clean part of the filter. *ATN* was calculated as:

$$ATN=100*\ln(I_0/I) \quad (6)$$

where I_0 and I are the light intensities transmitted throughout a reference blank spot and the aerosol-laden 3 mm diameter sample spot of the filter, respectively.

The attenuation coefficient of the particles collected on the filters, b_{ATN}, was derived from *ATN* as follows (Weingartner et al., 2003):

$$b_{ATN} = \frac{A}{100Q}\frac{\Delta ATN}{\Delta t} \quad (7)$$

where ΔATN indicates the *ATN* variation during the time period Δt, A is the sample spot area ($7.1 \cdot 10^{-6}$ m^2) and Q is the volumetric flow rate ($2.5 \cdot 10^{-6}$ m^3 sec^{-1}).

Finally, to determine the BC ambient concentration the apparent mass attenuation cross-section (σ_{ATN} = 12.5 m^2 g^{-1}) is needed; it is defined for the BC collected on the PTFE-coated borosilicate glass fiber filter and is provided by the manufacturer. The BC concentrations were determined as follows:

$$BC = \frac{b_{ATN}}{\sigma_{ATN}} \quad (8)$$

In addition to BC, the micro-Aethalometers allows also the determination of the aerosol absorption coefficient, b_{abs}, that was calculated as follows:

$$b_{abs} = \frac{b_{ATN}}{C \cdot R(ATN)} \quad (9)$$

where C and $R(ATN)$ are the multiple scattering optical enhancement factor and the aerosol loading factor, respectively. Briefly, the constant optical enhancement factor C compensates for the enhanced optical path through the filter caused by multiple scattering induced by the filter fibers themselves (Schmid et al., 2006; Arnott et al., 2005, Weingartner et al., 2003). For the AE51, and the prototype, the parameter C is 2.05 ± 0.03 (at λ = 880 nm) (Ferrero et al., 2011a). The parameter $R(ATN)$ compensates for the nonlinearity – the loading effect due to reduction of the measurement sensitivity due to the saturation caused by the collected sample on the filter. The compensation with the parameter $R(ATN)$ is needed only when *ATN* becomes higher than 20 (Schmid et al., 2006; Arnott et al., 2005; Weingartner et al., 2003). In this study, the experimental design allowed us to neglect the use of $R(ATN)$: all BC vertical profiles were conducted in the clean Arctic environment and the filter tickets were changed to always keep *ATN* lower than 20 as recommended by Weingartner et al. (2003).

Atmos. Chem. Phys. Discuss., doi:10.5194/acp-2016-171, 2016
Manuscript under review for journal Atmos. Chem. Phys.
Published: 13 April 2016

Atmospheric Chemistry and Physics Discussions

The accuracy of BC measured by the two instruments was investigated by comparing the AE51 and the prototype measurements carried out simultaneously both during some of the balloon flights and at ground during spring 2011. The result of this intercomparison is reported in Figure 2c; as shown, BC measurements obtained by the two micro-Aethalometers agreed very well (R^2=0.852; slope=0.976) with a RMSE of 2 ng m^{-3} (considering the average of the two measurements as the target value).

The above reported RMSE underlines a critical situation for summer BC determination because, as reported in Eleftheriadis et al. (2009), the BC concentration range expected in summer is ~0-10 ng m^{-3}. Thus, summer BC data were used here only to highlight the impact of shipping emissions on the Arctic background concentrations along the atmospheric column. Due to high ship impact (section 3.4), the performance of the micro-Aethalometers was suitable and reliable for the purpose of this application.

2.2.3 Meteorological data and aerosol stratifications

Meteorological data along height allowed the determination of the absolute height of the balloon using the hypsometric equation; due to change during April 2011 in the measuring system (section 2.2), a comparison of the altitude obtained by the LSI-Lastem and Vaisala tethersonde was conducted during several target flights. The result is shown in Figure 2d (R^2=0.997; slope=0.999) and demonstrates the accuracy of the height determination.

A proper altitude is fundamental in the study of the vertical aerosol properties in relationship with meteorological parameters. Usually, vertical aerosol profiles allows the determination of the Planetary Boundary Layer height (PBL_h) by means of a gradient method, applied to aerosol concentration profiles, as suggested by Seibert et al. (2000). The aerosols are used as tracer of atmospheric plumes integrating the effects of turbulent forces (thermal and mechanical) along height. The gradient method's ability to infer the PBL_h from aerosol vertical profiles has been demonstrated in previous works (Ferrero et al., 2012, 2011a, 2011b and 2007; Sangiorgi et al., 2011; Di Liberto et al., 2012), however, in remote areas, such the Arctic, several processes other than dispersion can shape the aerosol profiles. The two most important ones are: 1) differential advection (Tunved et al., 2013) and 2) a lack of emission of aerosol from ground. These processes should generate a vertical structure not directly related to the PBL_h. To avoid misinterpretations, the results of the gradient's method will be hereinafter indicated as Aerosol Stratification heights (AS_h) even if, as it will be addressed in secion 3.2, they are well related to the behaviour of meteorological variables governing the behaviour of the PBL_h.

The AS_h will be used in the next sections to calculate averaged aerosol and BC profiles (sections 3.3 and 3.4). In fact, in order to better investigate the variation of aerosol properties with height, vertical profiles were statistically averaged. As reported in previous works (Ferrero et al., 2011a, 2012 and 2014), a way to average vertical profile data by taking their main gradients (AS_h) into account, is to consider the relative position of each measured data point in respect to the AS_h. Thus, vertical profiles were first normalized, introducing a standardized height (H_s) calculated as follows:

$$H_s = \frac{z - AS_h}{AS_h} \quad (10)$$

where z is the height above ground. H_s assumes a value of 0 at the AS_h, and values of -1 and 1 at ground-level and at twice the AS_h, respectively.

Atmos. Chem. Phys. Discuss., doi:10.5194/acp-2016-171, 2016
Manuscript under review for journal Atmos. Chem. Phys.
Published: 13 April 2016

Atmospheric Chemistry and Physics Discussions

3 Results and Discussion

Aerosol and BC and vertical profiles were measured to assess changes in aerosol properties within the vertical column in the Arctic region. The results obtained along vertical profiles are discussed in order to highlight first the vertical behaviour of the AS_h in relation to the main atmospheric meteorological parameters (section 3.1 and 3.2). Then, vertical aerosol properties are discussed in details for springtime (section 3.3) and summertime (section 3.4). All averaged data are reported hereinafter as mean ± mean standard deviation.

3.1 Vertical profile data

As reported in Table 1, 200 profiles were measured during 3 campaigns in spring 2011, summer 2011 and summer 2012. Before to introduce the results, it is necessary to briefly describe the ambient conditions under which the vertical profiles were measured.

First of all, the observational periods (spring 2011, summer 2011 and summer 2012) were addressed in a climatological context. In this respect, Figure S1a-b show the daily mean temperature during the campaign periods (spring 2011, summer 2011 and summer 2012) in comparison to the 20-year longterm daily mean (1993-2014, excluding 2011 and 2012). Figure S1a shows a larger interannual springtime variability. Spring 2011 exhibited a temperature close to that measured on average on a 20-years period; just during the last 10 days the temperature was slightly higher. Figure S1b shows that both during summer 2011 and summer 2012, the temperature trend was close to that measured on the 20-years period. As a result, spring 2011, summer 2011 and summer 2012 can be considered typical for the local climatologic context. Thus, vertical profiles measurements were conducted under meteorological conditions representative of the reality of Ny-Ålesund.

It should be reminded, however, that the tethered balloon has limitations with respect to its launch conditions (section 2.2). Particularly, the maximum wind speeds registered at ground during balloon flights in spring 2011 and in summer 2011-2012, were 4.9 m s^{-1} and 10.7 m s^{-1}, lower than the absolute wind speeds registered during the same periods: 27.9 m s^{-1} and 16.3 m s^{-1}. Moreover, quite all measurements were conducted under clear sky conditions (no clouds) or with clouds whose base was higher than the maximum altitude reached by the balloon. The presence/absence of clouds and their base height were determined using the Vaisala LD-40 ceilometer (section 2.1.2). Table 1 resume the sky conditions for all the measured profiles. Clear sky conditions were dominant during the three campaigns.

Thus, it is possible to assert that the measured profiles, and the seasonal phenomenology described hereinafter, are representative of typical Arctic springtime and summertime periods mainly for low wind and clear sky conditions. In order to introduce now the obtained results, Figure 3a-d shows some examples of vertical aerosol profiles accompanied by the corresponding potential temperature (θ) and RH profiles.

From Figure 3a-d (and the whole ensemble of collected data), several information can be derived to accurately describe the vertical distribution of the aerosol and its properties in the first kilometre above Ny-Ålesund.

The first information that can be obtained, is the absence or the presence of marked aerosol stratifications (AS); when present, their altitude (AS_h) was determined through the used of a gradient method as described in section 2.2.3. With respect to this first information, while Figure 3a highlights a condition in which the aerosol was homogeneously distributed with altitude (due to a negative vertical gradient of θ), Figure 3b-d evidences marked concentration changes in agreement with the altitudes at which positive gradients for θ and negative gradients for RH were located.

Atmos. Chem. Phys. Discuss., doi:10.5194/acp-2016-171, 2016
Manuscript under review for journal Atmos. Chem. Phys.
Published: 13 April 2016

Atmospheric Chemistry and Physics Discussions

A second information obtained from the profiles was the size dependent vertical behaviour of aerosol concentrations. With respect to this, Figures3b and 3c highlight a similar behaviour for both $N_{14\text{-}260}$ and $N_{260\text{-}1200}$ while, Figure 3dshows a loss of symmetry between the two sizes ($N_{14\text{-}260}$ and $N_{260\text{-}1200}$) due to a concentration change located at a different altitude.

Finally, the third obtained information was the magnitude of the observed concentration change at each AS_h for each size range ($N_{14\text{-}260}$, $N_{260\text{-}1200}$and $N_{>1200}$) and season.

The analysis and combination of these three types of information allowed to unravel the following tasks:

1) at which altitude and with which frequency the aerosol stratifications were located over Ny-Ålesund in function of their size and season,

2) how intense were the concentration changes for each season and size,

3) what were the possible dynamics underlying the seasonal phenomenology found during the campaign.

The first task is discussed in the following section (3.2) while the measured concentration changes along height together with an explanation of the possible dynamics originating the observed seasonal phenomenology are discussed separately for spring (section 3.3) and summer (section 3.4). For the last task, BC profiles and ground-based aerosol chemistry and size distribution data were used.

3.2 Aerosol stratifications: seasonal vertical frequency distribution and relationship with meteorology

Figure 3a-d highlights different atmospheric dispersal conditions upon Ny-Ålesund. Although these four case studies are not illustrative and comprehensive of the whole data set, their discussion helps to illustrate the seasonal and size-dependent behaviour of the frequency distribution of the AS_h with altitude.

An example for homogeneous dispersion of aerosol (independent from its size) in the lower troposphere is shown in Figure 3a. Decreasing potential temperature with height indicates atmospheric instability, allowing the vertical mixing of air masses by convection. Homogeneous aerosol profiles with convective conditions were found in 15% of the profiles in spring and 37% of the profiles in summer, respectively. Although the statistics may be biased due to the launch conditions (low wind speed) for the tethered balloon (section 3.1), convective conditions generally are observed more frequent during summer in Ny-Alesund related to the different surface properties. Commonly in spring, the ground is still snow covered (with albedo values 0.87±0.04 in spring 2011) while, snow melt season occurs basically during the month of June, and July is usually snow-free, exposing the tundra ground (with albedo values 0.15±0.01) (Mazzola et al. 2015a). The resulting change in surface energy balance affects the atmospheric stability, from the more stable conditions and inversion situations with snow-cover to the unstable conditions favouring mixing within the boundary layer once the snow cover has disappeared.

The observed homogenous mixing conditions, when present, allowed us to assume that the aerosol properties measured at ground-level in Ny-Ålesund were representative for the lower troposphere.

More frequent than the homogeneous mixing conditions, the presence of different layers of aerosol, separated by abrupt changes in the aerosol properties (i.e. concentration) along height were observed (Figure 3b-d). The presence of aerosol stratification was complementary to the homogenous profiles and thus occurred for 85% and 63% of cases during spring and summer, respectively.

Within this conditions it was possible to determine the AS_h for each aerosol size and season together with the altitude of sharp changes observed also for θ and RH. For example, Figure 3c shows AS_h at 630 m in agreement with the vertical gradients of θ and RH. On the other hand, Figure 3d show a first AS_h at 134 m only for $N_{14\text{-}260}$,

Atmos. Chem. Phys. Discuss., doi:10.5194/acp-2016-171, 2016
Manuscript under review for journal Atmos. Chem. Phys.
Published: 13 April 2016

Atmospheric Chemistry and Physics Discussions

while $N_{260\text{-}1200}$ appeared homogenously distributed until a second AS_h located at 674 m; the first AS_h detected for the smallest particles was related to a ground-based θ inversion, while the second AS_h detected for the accumulation mode particles was related to an elevated θ inversion.

The aforementioned case studies are instructive to introduce the description of the AS_h frequency distribution with altitude and season. The AS_h were used independently from the sign of the aerosol concentration change (either positive or negative; Figure 3b-c) and were computed separately for each broad size range (i.e. Figure 3d). Moreover, it has to be underlined that, sometimes it was possible to detect up to two AS_h for each profile. This situation was observed for ~30%of profiles (characterized by the presence of aerosol gradients) in spring and summer, due to the limited maximum altitude reached by the balloon during the flight (usually between 0.7 and 1.3 km). In Ny-Alesund, an elevated inversion is frequently observed in relation to the surrounding mountains, orographic obstacles that keep the synoptic flow over the mountains separate from the inner-fjord boundary layer regime with local advection along the fjord axis. Here, the behaviour of the second AS_h (see Figure S2) is used below to support the description of the behaviour of the first aerosol stratification with altitude.

The resulting frequency distribution with altitude of the first AS_h is reported in Figures4a-d and Figures4e-h for spring and summer, respectively.

Focusing on each season and considering first the springtime AS_h vertical frequency distributions (Figure 4a-d) a common behaviour can be first observed for both the three broadsize ranges ($N_{14\text{-}260}$, $N_{260\text{-}1200}$ and $N_{>1200}$) and meteorological parameters (θ and RH): all of them showed a bimodal distribution characterized by a minimum within the ~400-500 m height range. As mentioned above, the surrounding mountains often cause a separation of the synoptic flow above and the inner-fjord regime an elevated inversion induced by differential advection. Thus, the observed separation of aerosol properties most likely relates to the separation of the atmospheric flow, with the lowermost part of the profiles being affected by local micrometeorology and the upper part characterized by the synoptic flow.

Moving forward, some differences were then found in the behaviour of each aerosol size range below and above the minimum at 400-500 m. While $N_{260\text{-}1200}$ and $N_{>1200}$ (Figure 4b-c) appeared equally distributed below and above the minimum at 400-500 m, $N_{14\text{-}260}$ showed highest frequencies of AS_h below 400 m (Figure 4a). Particularly, the 82% of AS_h for $N_{14\text{-}260}$ were located below 400 m and showed a clear maximum peak close to the ground (0-100 m) with a frequency of 38%. Moreover, the average values of AS_h for$N_{14\text{-}260}$ below and above the minimum at 400-500 m were 143±13 m and 669±32 m, respectively. Conversely, AS_h for $N_{260\text{-}1200}$ and $N_{>1200}$occurred for 52% and 51% below 400 m peaking in the 100-200 m range (22% and 21%, respectively) with average values of 208±19 m and 177±14 m, respectively. Above 400 m the AS_h for $N_{260\text{-}1200}$ and $N_{>1200}$ peaked in the 600-700 m range (22% and 19%, respectively) with average values of 672±16 m and 652±20 m.

The observed lack of symmetry between $N_{14\text{-}260}$ and $N_{260\text{-}1200}$– $N_{>1200}$ is explained in Figure 3d, where a decoupled trend for $N_{14\text{-}260}$ and $N_{260\text{-}1200}$ is shown. As stated above, the behaviour of smallest particles was in that case related to a ground-based θ inversion. Considering the whole data set, the behaviour of the vertical frequency distribution of the first gradient of both θ and RH was in agreement with that of AS_h for $N_{14\text{-}260}$; in this respect, a maximum peak for both θ and RH was found close to the ground (0-100 m) with a frequency of 49% and 38%, respectively (average values below the minimum at 400-500 m for gradients for θ and RH of 117±12 m and 669±32 m). Interestingly, the frequency of ground-based θ inversions (49%) was higher than that of AS_h for $N_{14\text{-}260}$ (38%); this feature is due to vertical profile along which, even in the presence of a ground-based θ inversion, $N_{14\text{-}260}$ did not

Atmos. Chem. Phys. Discuss., doi:10.5194/acp-2016-171, 2016
Manuscript under review for journal Atmos. Chem. Phys.
Published: 13 April 2016

show any variation of concentration; an example is reported in Figure3b.Thus, the presence of a ground-based θ inversion appears as a necessary but not sufficient condition to observe the aforementioned behaviours (resumed by Figure 3d, Figure 4a and 4d). In this, respect, the phenomenology and the aerosol dynamic responsible of this behaviour (together with that of $N_{260\text{-}1200}$– $N_{>1200}$) will be addressed and discussed in the following section 3.3.

Here below, the summer AS_h behaviour is described. Figure 4e-h (and Figure S1) show that, even in summer, the multi-layered structure persisted and was also characterized by a bimodal distribution, as in spring, but with with a higher minimum (than in spring) that ranged approximately between 500 m and 600 m.

With respect to this, the summer AS_h for all size ranges and the gradient for θ and RH peaked between 100 and 300 m: 78% ($N_{14\text{-}260}$; average value 276±19 m),71% ($N_{260\text{-}1200}$; average value 269±18 m), 76% ($N_{>1200}$; average value 272±18 m), 83% (θ; average value 262±18 m) and 79% (RH; average value 268±18 m).

Figure 4e-h, and the aforementioned data, highlight that the vertical frequency distribution for AS_h of all sizes and gradients for θ and RH behave similarly. This phenomenon, different from that observed in spring, will be addressed and discussed in section 3.3.

As a final conclusion, a multi-layered structure was found over Ny-Ålesund both in spring and summer (see also Figure S1), and the most important atmospheric thermodynamic parameters (θ and RH) indicated the role of meteorology in shaping the aerosol vertical profiles. This result is of great importance as the majority of the aerosol measurements conducted in the Arctic area are ground-based and thus, it is necessary to understand their validity with altitude.

Here below, the observed vertical aerosol phenomenology is discussed separately for spring (section 3.3) and summer (section 3.4).

3.3 Springtime phenomenology

The previous section (3.2) introduced the vertical behaviour of sized aerosol in terms of frequency distribution of AS_h. However, it is also necessary to describe the intensity of the aerosol concentration changes at the AS_h, and the possible dynamics underlying these changes. Thus in this section, the springtime vertical aerosol phenomenology will be investigated.

In this respect, all the profiles measured in spring 2011 were classified on the basis of their vertical behaviour (i.e. shape) and averaged considering the relative position of each measured data point with respect to the AS_h. The obtained averaged vertical profiles were referred to a standardized height (H_s, Eq. 10) as described in section 2.2.3. As the size classes can behave differently with height, H_s=0 was referred to that observed for the intermediate $N_{260\text{-}1200}$ size class.

The result of the classification and averaging procedure is reported in Figure 5a-h, where the four main typologies of springtime aerosol behaviour are shown for both the three broadsize ranges ($N_{14\text{-}260}$, $N_{260\text{-}1200}$, $N_{>1200}$) and also BC concentrations.

According to their shape they were named as follows:

1) Type 1, homogeneous profiles (hereinafter addressed as HO), Figure 5a-b

2) Type 2, profiles characterized by a positive gradient at AS_h=0 (hereinafter addressed as PG), Figure 5c-d

3) Type 3, profiles characterized by a negative gradient at AS_h=0 (hereinafter addressed as NG), Figure 5e-f

4) Type 4, profiles characterized by negative gradients located ad different altitude in function of size (hereinafter addressed as decoupled negative gradient, DNG), Figure 5g-h.

Atmos. Chem. Phys. Discuss., doi:10.5194/acp-2016-171, 2016
Manuscript under review for journal Atmos. Chem. Phys.
Published: 13 April 2016

Atmospheric Chemistry and Physics Discussions

Prior to discuss each profile class separately, it is worth noting to briefly report the columnar averages of both total aerosol number and BC concentrations obtained by averaging the aforementioned profile classes: 236.1±23.9 cm^{-3} (N_{14-260}), 21.1±1.3 cm^{-3} ($N_{260-1200}$), 0.2±4*10^{-2} cm^{-3} ($N_{>1200}$) and 52±8 ng m^{-3} (BC). They perfectly agree with long-term data series collected over Ny-Ålesund at the Zeppelin observatory (Eleftheriadis et al., 2009a; Tunved et al., 2013) during Spring. This indicates that all the profile classes discussed here below influence (with their occurring frequencies and altitudes) the background Arctic aerosol measured by strategic Arctic observatories.

Finally, the CCT wind data were used to compute wind rose graphs timely coincident with each profiles typology (Figure 7a-d). Results evidenced the absence of wind from north during the profiles, thus avoiding any influence from Ny-Ålesund. The profile typology observed during each day of campaign is reported is summarized in Table 1.

3.3.1 Homogeneous Profiles (HO)

HO profiles (Type1, Figure 5a-b) were observed in 15% of cases (during 7 days) and described homogenous vertical distribution of aerosol and BC upon Ny-Ålesund. These are the only profiles referred to an absolute height AGL, due to the fact that they did not show any AS_h to calculate H_s. As also shown in Figure 3a, negative θ gradient allowing vertical mixing favoured this typology of profiles in which the aerosol pollution, previously transported from mid-latitudes, affected the first km of the atmosphere. The aerosol number concentrations were found to be 80.2±16.4 cm^{-3} (81.9±16.8% of the total aerosol concentration), 17.5±2.0 cm^{-3} (17.9±2.0% of the total aerosol concentration) and 0.2±0.1 cm^{-3} (0.2±0.1% of the total aerosol concentration) for N_{14-260}, $N_{260-1200}$, $N_{>1200}$, respectively. The aerosol number concentration was thus dominated by the N_{14-260} size fraction along the whole profile. BC and the related b_{abs} (section 2.2.2, eq. 4) reached values of 35±21 ng m^{-3} and 0.22±0.13 Mm^{-1}.

3.3.2 Positive Gradient Profiles (PG)

PG profiles (Type 2, Figure 5b-c) occurred in 17% of cases (during 6 days) and were characterized by an increase of aerosol number concentrations above H_s=0 and moderate BC concentrations (24±3 ng m^{-3}; b_{abs} was 0.14±0.02 Mm^{-1}). The increment of aerosol number concentrations with altitude was particularly evidentforN_{14-260}that increased by +171.5±25.4% (going from 205.4±12.5 cm^{-3} below the AS_h to 557.6±45.9 cm^{-3} above it) while, $N_{260-1200}$ experienced a more modest increase of 11.8±7.0% (going from 19.9±0.2 cm^{-3} below the AS_h to 22.3±1.4 cm^{-3} above it). Conversely, the coarse fraction ($N_{>1200}$) decreased with altitude of -38.1±10.0% (going from 0.26±0.02 cm^{-3} below the AS_h to 0.16±0.02 cm^{-3} above it). The observed increase of Aitken and Accumulation mode fractions (N_{14-260} plus $N_{260-1200}$), and the corresponding decrease of the coarse fraction ($N_{>1200}$) appears in agreement with the observation that during transport events wet removal processes decrease the coarse particle concentration by scavenging and, at the same time, this establish conditions that favour secondary aerosol formation due to the lowering of the condensational sink (Tunved et al., 2013). Thus, the PG profile data suggested that high altitude transport events could be the origin of this type of profiles during springtime. An example of this process is given by the interesting case study of 23th April 2011 (1200-1330 UTC), when an intense plume of aerosol was transported over Ny-Ålesund; Figure 6a-b shows this event coupling air mass back trajectories and the time evolution of the event obtained through the interpolation of 6 vertical profiles, each of which lasted ~15 min and was distanced ~1 min from the following profile.

Atmos. Chem. Phys. Discuss., doi:10.5194/acp-2016-171, 2016
Manuscript under review for journal Atmos. Chem. Phys.
Published: 13 April 2016

Atmospheric Chemistry and Physics Discussions

High aerosol concentrations at high altitude are important because aerosols can act as CCN and thus impact on climate via the indirect aerosol effects.

3.3.3 Negative Gradient Profiles (NG)

NG profiles were observed in 48% of all cases (during 9 days) making the NG the dominant typology of profiles. In this respect, figure 6b not only showed the origin of a PG profile, but interestingly also showed that, after the arrival, the transported aerosol was mixed downward within the PBL until ground. Most important, at the end of the process (1330 UTC) a negative concentration gradient with altitude was established generating a NG profile.

As now shown, NG profiles (Figure 5e-f) might be originated from the entrance of Arctic Haze into the PBL after a transport process. In the Arctic, in absence of an important local aerosol source (i.e. nucleation which acts mainly in summer as reported in Tunved et al. (2013)), only transported aerosol trapped within a thermal inversion made possible the presence of this typology of profiles. The presence of a intense θ inversion stabilizes the situation maintaining a NG typology of profile since vertical mixing is prevented; an example is shown in Figure 3c. It has to be noticed that an intense θ inversion is just a necessary condition to promote the formation of NG profiles, not a sufficient one. As yet described in section 3.2.1, the frequency of ground-based θ inversions (49%, Figure 4d) reached values higher than those for any AS_h for any aerosol size (Figure 4a-c).

Once established, NG profiles were characterized by high pollution levels below H_s=0 where an intense decrease of both aerosol and BC was observed. Crossing the AS_h, aerosol concentrations decreased by -52.9±8.7% (from 252.3±17.5cm^{-3} to 118.9±9.3cm^{-3}) for $N_{14\text{-}260}$, by -57.9±2.6% (from 23.1±0.4cm^{-3} to 9.7±0.3 cm^{-3}) for $N_{260\text{-}1200}$ and by -66.5±11.5% (from 0.53±0.05cm^{-3} to 0.18±0.02cm^{-3}) for $N_{>1200}$. BC behave similarly decreasing by -50.4±6.8% (from 71±4 ng m^{-3} to 35±2 ng m^{-3}) and the same happened to b_{abs} (from 0.43±0.02Mm^{-1} to 0.21±0.01Mm^{-1}). The last finding is very important because, as the altitude of BC occurrence in the atmosphere modulates its influence on the climate in the Arctic.

3.3.4 Decoupled Negative Gradient Profiles (DNG)

A particular kind of profiles characterized by a decrease in concentration with altitude is the DNG typology. Within this class, observed in 20% of cases (during 5 days), a lack of symmetry between $N_{14\text{-}260}$ and $N_{260\text{-}1200}$– $N_{>1200}$can be observed (Figure 5g-h).

Particularly, $N_{14\text{-}260}$ showed a concentration peak close to the ground of 601.3±19.9 cm^{-3} that was not present for $N_{260\text{-}1200}$ and $N_{>1200}$; $N_{260\text{-}1200}$ and $N_{>1200}$ instead remained quite constant (32.4±0.8 cm^{-3} and 0.17±0.01 cm^{-3}, respectively) from ground until H_s=0.

$N_{14\text{-}260}$ quickly decreased above the ground-based peak (-58.6±4.3%) to a concentration value of 249.0±11.5 cm^{-3} analogous to that observed in standard NG profiles (252.3±17.5 cm^{-3}) below the AS_h (before reaching H_s=0). Then, at H_s=0, all the three broadsize ranges decreased; on average by -54.4±6.2% (from 249.0±11.5 cm^{-3} to 113.5±8.2 cm^{-3}) for $N_{14\text{-}260}$, by -31.1±2.9% (from 32.4±0.8 cm^{-3}to 22.3±0.8 cm^{-3}) for $N_{260\text{-}1200}$ and by -54.2±4.7% (from 0.17±0.01 cm^{-3} to 0.08±0.01 cm^{-3}) for $N_{>1200}$. Thus, above H_s=0, all the three broadsize classes behave similarly to those described in standard NG profiles. Interestingly, BC concentrations behave contrary to the $N_{14\text{-}260}$ aerosol fraction. Particularly, lowest BC concentrations were found close to the ground (36±11 ng m^{-3}; b_{abs} was 0.22±0.06 Mm^{-1}) in correspondence of the $N_{14\text{-}260}$ concentration peak; above this peak, BC concentrations were higher (101±5

Atmos. Chem. Phys. Discuss., doi:10.5194/acp-2016-171, 2016
Manuscript under review for journal Atmos. Chem. Phys.
Published: 13 April 2016

Atmospheric Chemistry and Physics Discussions

ng m^{-3}; b_{abs} was 0.62±0.03 Mm^{-1}) and more close to that observed in standard NG profiles at altitudes below H_s=0.Then, above H_s=0, also BC decreased (-22.5±9.7%).

All the aforementioned observations suggest that a particular process could have influenced ground-level concentrations for this size class only. In order to shade light on this process several parameters will be here below considered, namely: meteorological parameters, the aerosol chemical composition and the aerosol number size distribution.

Starting with meteorological parameters, and recalling first Figure 3d, it is possible to assess that the behaviour of smallest particles in the proximity of the ground can be observed concomitantly to the presence of ground-based θ inversions. A necessary condition (or a concurrent cause) to promote the presence of ground-based concentration peaks for $N_{14\text{-}260}$; the crucial point to unravel this phenomenon is to understand the possible origin of this particles. Thus, ground-based aerosol and meteorological measurements, collected at Gruvebadet laboratory and at the CCT (section 2.1) and temporally coincident with the observation of DNG profile, were considered.

Figure 8a-d first resumes the ground-level PM_{10} chemical composition determined for the four categories (HO, PG, NG, DNG) of profiles; the total sulphate fraction in DNG profiles (26.2±2.4%) was double than that observed in the other profile classes: 11.5±2.3%, 12.0±2.6% and13.9±3.0% for HO, PG and NG, respectively. Most important, the nss-nc-SO_4^{2-}fraction (determined as reported in section 2.1.1) in DNG profiles (24.3±2.5%) was 2.4±0.4 times higher than that observed in the other profile classes (9.6±2.3%, 9.4±2.7% and 11.5±3.1%, for HO, PG and NG, respectively) while both the ss-SO_4^{2-} and the cr-SO_4^{2-} fractions remained quite constant and during the DNG profiles were both 0.8±0.4 times than that observed in the other profile classes (HO, PG and NG, respectively). These observations, coupled with the lowering of BC fraction in proximity of the ground (Figure 5g) points towards the hypothesis that the ground-based $N_{14\text{-}260}$ concentration peak was due to secondary origin. The nss-nc-SO_4^{2-} fraction during DNG profiles appeared in acidic form as it was just poorly neutralized by the ammonium. Particularly, the w/w (weight/weight) nss-nc-SO_4^{2-}/NH_4^+ ratio was 1.6±0.4 times higher in DNG profiles (10.3±1.5) than that observed in the other profile classes: 6.1±1.9,5.8±2.1 and7.0±2.2 for HO, PG and NG, respectively. As reported in literature (Udisti et al., 2015; Becagli et al., 2012; Udisti et al., 2012) these values for DNG profiles evidenced the presence of sulphate in acidic form (H_2SO_4). This information is very important when coupled with meteorological data measured at the CCT (Table 2). Focusing first on the air temperature, it can be observed that, during DNG profiles, the temperature close to the ground (-17.2±0.3 °C) was lower than that observed in the other profile classes: -9.7±0.5 °C, -5.9±0.3 °C and -9.9±0.2 for HO, PG and NG, respectively. In addition, the RH was 18.0±2.0% higher (73.6±0.3%) in DNG profiles, compared to that observed in the other profile classes. Finally, also the wind speed during DNG profiles was half than during the other profile classes and was not affected by north direction avoiding the influence of Ny-Ålesund (Figure 7d).

All the aforementioned conditions can be resumed here in: higher acidic sulphate fraction, lower BC fraction, lower temperature, higher relative humidity and lower wind speed during DNG profiles.

As reported in literature (Kirkby et al., 2011; Reddington et al., 2011;Lovejoy et al., 2004) these conditions decrease the height of the barrier for new particle formation just considering the very simplified binary H_2SO_4–H_2O system. Under these conditions, the secondary aerosol formation can proceed at ambient acid concentrations in the cooler mid-troposphere and at lower altitude in polar regions. However, it has to be underlined that, as recently reported (Riccobono et al., 2014), organics plays a fundamental role for secondary aerosol formation.

Atmos. Chem. Phys. Discuss., doi:10.5194/acp-2016-171, 2016
Manuscript under review for journal Atmos. Chem. Phys.
Published: 13 April 2016

Atmospheric Chemistry and Physics Discussions

They were found in Ny-Ålesund even in spring (Zangrando et al., 2013). These figures, coupled with the aforementioned data indicated the $N_{14\text{-}260}$ concentration peaks at ground as locally formed secondary aerosol.

The ground-based aerosol number size distribution measured at Gruvebadet (section 2.1) was reported in Figure 9 for HO, PG, NG and DNG profiles, respectively. A huge Aitken mode is clearly visible for DNG profiles, while it is negligible for the other profile classes. This mode was characterized by a geometric mean diameter D_g of 0.032±0.001 μm and by a geometric standard deviation σ_g of 1.790±0.006 that were in agreement with ten-year average values reported in Tunved et al. (2013) at the Zeppelin observatory during the month of April. The presence of a clearly visible Aitken mode in DNG profiles supports the aforementioned hypothesis of the presence of a ground-based plume of locally formed secondary aerosol.

With respect to this, in order to estimate (meaning the order of magnitude) the contribution of locally formed aerosol, a simple method based on the N/BC ratio, developed by Rodríguez and Cuevas (2007) and successfully applied in Europe by (Reche et al., 2011) was used. The basic concept of this method is that highest values of N/BC ratios (i.e. the lowest BC fraction values) occur during secondary aerosol formation in the atmosphere (Reche et al., 2011; Dall'Osto et al., 2013 and 2011). The methodology is as follows:

$$N2 = N - N1 \quad (11)$$

$$N1 = S1 \times BC \quad (12)$$

where N2 represents the secondary aerosol concentration locally formed in the atmosphere, N is the measured aerosol number concentration and N1 is the aerosol number concentration yet present in the background air; N1 is calculated from the parameterS1multiplied by the measured BC concentration. S1represents a reference value for the N/BC ratio (expressed as particles $cm^{-3}/ng\ m^{-3}$ of BC)in the background air. S1 can vary from ~2 to ~9, while the N/BC ratio during secondary aerosol formation reaches values higher than ~15-20 and up to ~100-200 (Reche et al., 2011; Dall'Osto et al., 2013 and 2011). The differences in S1 values determined in different sites can be caused by: 1) the use of different particle counters (with different d_{50} cutoff), as lowest S1 values are usually observed when devices with largest d_{50}cutoff are used; 2) the influence of the ambient air conditions on the secondary aerosol formation.

Thus, S1 is site-instrument specific and has to be determined on-site depending on the used particle counter. If the Rodríguez and Cuevas (2007) method is applied to ground-based temporal data series, S1 can be obtained as the minimum N vs. BC slope observed during the day (Reche et al., 2011). However, in the case of measured vertical profiles, the values of S1 were taken as that of background aerosol above the ground $N_{14\text{-}260}$ plume in DNG profiles; the obtained S1 value was 2.4±0.2.This value was very similar to that measured during HO profiles (2.5±0.1) when a pure background aerosol was measured. It can be observed that these S1 values obtained over Ny-Ålesund are close to the lowest values reported in literature (Reche et al., 2011; Dall'Osto et al., 2013); this is simply due to the d_{50} cutoff size of the miniDiSC (14 nm; section 2.2.1) which is higher than d_{50} cutoff sizes (~2-7 nm) usually present on the widely used condensation particle counters.

Using this reference S1 value (2.4±0.2), N1 (background number concentration) and N2 (locally formed secondary aerosol) were computed. Their vertical behaviour is reported in Figure 10 where the total amount of secondary aerosol close to the ground is clearly visible and accounted on average for 63.7±5.6% (up to 95% at ground) of the total $N_{14\text{-}260}$ plume measured during DNG profiles. In fact, within these plumes, the $N_{14\text{-}260}$/BC ratio reached an average value of 22.5±5.4 (maximum value of 54.8 at ground) clearly indicating, as reported in Reche et al. (2011) and in Dall'Osto et al. (2013) the presence of a secondary formed aerosol.

Atmos. Chem. Phys. Discuss., doi:10.5194/acp-2016-171, 2016
Manuscript under review for journal Atmos. Chem. Phys.
Published: 13 April 2016

Atmospheric Chemistry and Physics Discussions

In addition to this, Figure 11 shows the temporal behaviour of SMPS+APS data collected at Gruvebadet during April 2011 together with the percentiles (25°, 50°, 75°, 90°) of the measured number size distribution. It is clearly evident the presence of nanoparticles (below 100 nm) even in Spring in the Arctic.

These findings point towards the importance of measuring the frequencies of these episodes in the future together with their vertical development (i.e. vertical mixing) to understand their importance in acting as CCN influencing the Arctic climate.

3.4 Summer phenomenology

As done in the previous section (3.3), also vertical profiles measured during summers 2011-2012 were classified in function of their vertical behaviour (i.e. shape) and averaged considering the relative position of each measured data point with respect to the AS_h. Even in this case, the obtained averaged vertical profiles were referred to the standardized height H_s.

The result of the classification and averaging procedure is reported in Figure 12a-d.

In summer, two main categories were observed:

1) Type 1, homogeneous profiles (HO), Figure 12a-b

2) Type 2, profiles characterized by the presence of meaningful impact of ship emissions (hereinafter addressed as SP), Figure 12c-d.

3.4.1 HO profiles

HO profiles (Type1, Figure 12a-b) were observed in 37% of cases due to the summer higher solar energy at disposal together with the low albedo as discussed in section 3.2. As already reported for springtime results, these are the only averaged profiles referred to an absolute height AGL due to the fact that they did not showed any AS_h to calculate H_s.

The aerosol number concentrations were found to be 435.9±5.8 cm^{-3} for $N_{14\text{-}260}$, 2.1±0.1cm^{-3} for $N_{260\text{-}1200}$, and $4*10^{-2}$±$4*10^{-3}$ cm^{-3} for $N_{>1200}$, respectively. Thus, $N_{14\text{-}260}$ accounted for 99.5±1.9% of the total aerosol number concentration, which is considerably higher than81.9±16.8% observed in springtime HO profiles. This is in agreement with the observations, reported in literature, that the sunlit summer period is dominated by small locally formed Aitken particles (Giardi et al., 2015; Tunved et al., 2013; Ström et al., 2009 and 2003; Udisti et al., 2013; Viola et al., 2013). BC and the related b_{abs} were negligible, as also reported by Eleftheriadis et al. (2009), and below the sensitivity of the micro-Aethalometer AE51.

HO profiles were observed in absence of ships anchoring in the harbour of Ny-Ålesund and when wind blew mainly from SW directions (Figure 7e).

3.4.2 Ship impact along vertical profiles

Summer vertical profiles showed a considerable impact of ship emissions. In these cases, wind blew mainly from the N-NE direction (where the harbour is located; Figure 7f) concomitantly with ships arrivals in the harbour of Ny-Ålesund. The number of ships and the number of passengers (a useful proxy of the ship dimension) was registered by the Kings-Bay Kull Company and it is reported in Figure S3 for summer 2011 and 2012, respectively. Particularly, 57 days with a total of 103 ship arrivals were registered during JJA of 2011 (62% of days; Figure 13a) while 78 days (85% of days) with 138 ships (Figure 13b) were registered during JJA of 2012.

Atmos. Chem. Phys. Discuss., doi:10.5194/acp-2016-171, 2016
Manuscript under review for journal Atmos. Chem. Phys.
Published: 13 April 2016

Atmospheric Chemistry and Physics Discussions

Figure 13a-e reports the case study of 6th July 2011, when four ships anchored (not simultaneously) in the harbour of Ny-Ålesund from 0700 UTC to 1900 UTC. The main ship arrived in the morning with approx. 1000 passengers. Figure 13a-e shows four profiles (0740 UTC, 0901 UTC, 0932 UTC and 1340 UTC; Figure 13a-d) together with ground SMPS data collected at Gruvebadet (Figure 13e); the ship impact in the Kongsfjord is clearly evident. N_{14-260} concentrations reached values up to 2-3*10^4 cm^{-3} and the BC concentrations reached the maximum value of 2000 ng m^{-3} (at 0932 UTC). Moreover, Figure 13a-d clearly showed that the ship plume was constrained below a AS_h that was lifted during the day (from 103 m to 592 m). Thus, the ship plume was constrained from ground to an altitude variable with time.

To highlight the impact of ship emission along the two years, average vertical profiles were calculated. The result is shown in Figure 12c-d. Once a ship plume arrived, SP profiles were characterized by high pollution levels below H_s=0. Particularly, N_{14-260} showed a concentration peak close to the ground of 9.0*10^3±2.5*10^2 cm^{-3}, $N_{260-1200}$ of 7.0±0.7 cm^{-3} and $N_{>1200}$ of 6*10^{-2}±4*10^{-3} cm^{-3}. BC behave similarly reaching concentrations of 319±14 ng m^{-3}. These concentration values were higher by a factor of 13.9±0.7 (N_{14-260}), 5.1±0.5 ($N_{260-1200}$), 4.8±0.4 ($N_{>1200}$) and 13.4±1.0 (BC) than those observed above H_s=0 where an intense decrease of both aerosol and BC is observed. Crossing the AS_h, aerosol concentrations decreased to 648.1±27.3 cm^{-3} for N_{14-260}, to 1.4±0.1 cm^{-3} for $N_{260-1200}$ and to 1*10^{-2}±1*10^{-3} cm^{-3} for $N_{>1200}$. These values were close to the background values observed during summer HO profiles. BC behave similarly decreasing to 24±1 ng m^{-3}.

As the ship plume of BC is located close to the ground, it may induce a positive forcing (Flanner, 2013; Brock et al., 2011; Seinfeld and Pandis, 2006; Hansen and Nazarenko, 2004). In fact, the b_{abs} reached values of 2.0±0.1 Mm^{-1} below H_s=0.

It is important to note that SP profiles were observed for the majority of cases in summer. In summertime the long-range transport of aerosol from midlatitudes is generally forbidden (Quinn et al., 2008). and the locally formed aerosol becomes in summer (Giardi et al., 2015; Tunved et al., 2013; Ström et al., 2009 and 2003). However, the SP profiles show that the reasing shipping emissions in the Arctic (Corbett et al., 2010; Granier et al., 2006) could affect the concentrations and the vertical distribution of aerosol, resulting in a positive forcing, induced by a positive feedback through the local anthropogenic impact on climate even in the summer.

4 Conclusions

Vertical profiles of in situ aerosol number size distribution and black carbon measurements were conducted by tethered balloon in the atmosphere over Ny-Ålesund. The balloon payload was equipped with an Optical Particle Counter (31 size classes, 0.25 to 32 μm), a electrical particle detector (d_{50}=14 nm), two micro-Aethalometers and a meteorological sensor. Moreover, chemical analysis of filter samples, aerosol size distribution and a full set of meteorological parameters at ground were available.

A systematic study of vertical profiles of aerosol number size distribution (14 nm – 32 μm) and black carbon concentrations was conducted allowing to collect more than 200 vertical profiles measured during spring and summer along 2 years (2011-2012). Using the collected experimental data vertical aerosol profiles were classified for each season according to their shape allowing to obtain a description of the seasonal phenomenology of vertical aerosol properties in the Arctic.

Focusing on spring, four main types of profiles were found.

The first one was the homogeneous profiles class, characterized by constant aerosol and BC concentration with altitude, and representative of Arctic background conditions.

The second class was that of positive gradient profiles characterized by an increase of aerosol concentration with altitude. The importance of this class is related to the fact that aerosols can act as CCN influencing the cloud cover and thus the longwave fluxes.

The third class was characterized by negative gradient profiles with a decrease of aerosol concentration with altitude and thus high pollution level close to the ground. This finding is very important because a BC layer located immediately above snow and ice may induce a positive forcing.

The fourth class of profiles was characterized by negative gradients located at different altitude in function of size. These profiles were observed during ground-based plume events of locally formed secondary aerosol. It is important as locally formed aerosol can act as CCN. As low clouds play a particular role in the sensitive Arctic climate system, the aerosol-cloud interactions will be one focus of future research activities within the Ny-Ålesund research community, manifested in the Ny-Ålesund Atmospheric Flagship program.

During summer, two main types of profiles were observed.

The first class was characterized by homogeneous background condition profiles while the second class reflected the impact of shipping emissions. During these episodes, a plume of aerosol and BC pollution was constrained close to the ground. In summer, atmospheric transport from midlatitudes is minor, an increasing shipping emission in the Arctic could significantly increase anthropogenic aerosol and BC concentrations in the summer Arctic, enhancing the climate change that this region is already experiencing.

Acknowledgements

The scientific activity in Ny Alesund was carried out in the framework of the CNR Polar Program. We thank the PRIN2009 “ARCTICA” project for financial support. We thank the Alfred Wegener Institute and the CICCI project for logistical support. We thank both Brent Holben and Piotr Sobolewski for their effort in establishing and maintaining the AERONET Hornsund site. Finally, we thank LSI-Lastem and Federico Pasquini for the cooperation concerning meteorological instruments.

References

Arnott, W. P., Hamasha, K., Moosmüller, H., Sheridan, P. J. and Ogren, J. a.: Towards Aerosol Light-Absorption Measurements with a 7-Wavelength Aethalometer: Evaluation with a Photoacoustic Instrument and 3-Wavelength Nephelometer, Aerosol Sci. Tech., 39(1), 17–29, doi:10.1080/027868290901972, 2005.

Ban-Weiss, G. a., Cao, L., Bala, G. and Caldeira, K.: Dependence of climate forcing and response on the altitude of black carbon aerosols, Climate Dynamics, 38(5-6), 897–911, doi:10.1007/s00382-011-1052-y, 2011.

Baron, P.A., and Willeke, K.: Aerosol measurements. Principles, Techniques and Applications. Wiley-Interscience, Second edition, 2005.

Bates, T. S., Quinn, P. K., Johnson, J. E., Corless, a., Brechtel, F. J., Stalin, S. E., Meinig, C. and Burkhart, J. F.: Measurements of atmospheric aerosol vertical distributions above Svalbard, Norway, using unmanned aerial systems (UAS), Atmospheric Measurement Techniques, 6(8), 2115–2120, doi:10.5194/amt-6-2115-2013, 2013.

Becagli S., Ghedini, C., Peeters, S., Rottiers, A., Traversi, R., Udisti, R., Chiari, M., Jalba, A., Despiau, S., Dayan, U., Temara, A.:MBAS (Methylene Blue Active Substances) and LAS (Linear Alkylbenzene Sulphonates) in Mediterranean coastal aerosols: sources and transport processes. Atmos. Environ., 45, 6788-6801, 2011.

Becagli, S., Scarchilli, C., Traversi, R., Dayan, U., Severi, M., Frosini, D., Vitale, V., Mazzola, M., Lupi, A., Nava, S., Udisti, R.:Study of present-day sources and transport processes affecting oxidised sulphur compounds in atmospheric aerosols at Dome C (Antarctica) from year-round sampling campaigns. Atmos. Environ., 52, 98-108, 2012.

Bhatt, U.S., Walker, D.A., Raynolds, M.K., Comiso, J.C., Epstein, H.E., Gia, G.-S., Gens, R., Pinzon, J.E., Tucker, C.J., Tweediw, C.E., Webber, P.J.: Circumpolar Arctic tundra vegetative change is linked to sea ice decline. Earth Interact. 14, 1–20, 2010.

Bowen, H.J.M.: Environmental Chemistry of the Elements. Academic Press, London,1979.

Brock, C. a., Cozic, J., Bahreini, R., Froyd, K. D., Middlebrook, a. M., McComiskey, a., Brioude, J., Cooper, O. R., Stohl, a., Aikin, K. C., de Gouw, J. a., Fahey, D. W., Ferrare, R. a., Gao, R.-S., Gore, W., Holloway, J. S., Hübler, G., Jefferson, a., Lack, D. a., Lance, S., Moore, R. H., Murphy, D. M., Nenes, a., Novelli, P. C., Nowak, J. B., Ogren, J. a., Peischl, J., Pierce, R. B., Pilewskie, P., Quinn, P. K., Ryerson, T. B., Schmidt, K. S., Schwarz, J. P., Sodemann, H., Spackman, J. R., Stark, H., Thomson, D. S., Thornberry, T., Veres, P., Watts, L. a., Warneke, C. and Wollny, a. G.: Characteristics, sources, and transport of aerosols measured in spring 2008 during the aerosol, radiation, and cloud processes affecting Arctic Climate (ARCPAC) Project, Atmospheric Chemistry and Physics, 11(6), 2423–2453, doi:10.5194/acp-11-2423-2011, 2011.

Browse, J., Carslaw, K. S., Schmidt, a. and Corbett, J. J.: Impact of future Arctic shipping on high-latitude black carbon deposition, Geophysical Research Letters, 40(16), 4459–4463, doi:10.1002/grl.50876, 2013.

Corbett, J. J., Lack, D. a., Winebrake, J. J., Harder, S., Silberman, J. a. and Gold, M.: Arctic shipping emissions inventories and future scenarios, Atmospheric Chemistry and Physics, 10(19), 9689–9704, doi:10.5194/acp-10-9689-2010, 2010.

Dai C.Y., Gao Z.Q., Wang Q., Cheng G. : Analysis of atmospheric boundary layer height characteristics over the Arctic Ocean using the aircraft and GPS soundings. Atmos. Oceanic Sci. Lett. 4: 124, 2011.

Dall'Osto, M., Thorpe, A., Beddows, D. C. S., Harrison, R. M., Barlow, J. F., Dunbar, T., Williams, P. I., and Coe, H.: Remark- able dynamics of nanoparticles in the urban atmosphere, At- mos. Chem. Phys., 11, 6623–6637, doi:10.5194/acp-11-6623- 2011, 2011.

Dall'Osto, M., Querol, X., Alastuey, A., O'Dowd, C., Harrison, R. M., Wenger, J. and Gómez-Moreno, F. J.: On the spatial distribution and evolution of ultrafine particles in Barcelona, Atmospheric Chemistry and Physics, 13(2), 741–759, doi:10.5194/acp-13-741-2013, 2013.

Di Liberto doi:10.1155/2012/851927...

Eckhardt, S., Stohl, a., Beirle, S., Spichtinger, N., James, P., Forster, C., Junker, C., Wagner, T., Platt, U. and Jennings, S. G.: The North Atlantic Oscillation controls air pollution transport to the Arctic, Atmospheric Chemistry and Physics Discussions, 3(3), 3222–3240, doi:10.5194/acpd-3-3222-2003, 2003.

Eckhardt, S., Hermansen, O., Grythe, H., Fiebig, M., Stebel, K., Cassiani, M., Baecklund, a. and Stohl, a.: The influence of cruise ship emissions on air pollution in Svalbard – a harbinger of a more polluted Arctic?, Atmospheric Chemistry and Physics, 13(16), 8401–8409, doi:10.5194/acp-13-8401-2013, 2013.

Eleftheriadis, K., Vratolis, S. and Nyeki, S.: Aerosol black carbon in the European Arctic : Measurements at °

lesund , Svalbard from 1998 – 2007 Zeppelin station , Ny-A, , 36, 0–4, doi:10.1029/2008GL035741, 2009a.

Eleftheriadis, K., Vratolis, S. and Nyeki, S.: Aerosol black carbon in the European Arctic: Measurements at Zeppelin station, Ny-Ålesund, Svalbard from 1998-2007, Geophysical Research Letters, 36(2), n/a–n/a, doi:10.1029/2008GL035741, 2009b.

Engvall, A., Krejci, R. and Str, J.: and Physics Changes in aerosol properties during spring-summer period in the Arctic troposphere, , 445–462, 2008a.

Engvall, A.-C., Krejci, R., Ström, J., Minikin, A., Treffeisen, R., Stohl, A. and Herber, A.: In-situ airborne observations of the microphysical properties of the Arctic tropospheric aerosol during late spring and summer, Tellus B, 080414161623888–???, doi:10.1111/j.1600-0889.2008.00348.x, 2008b.

Ferrero, L., Bolzacchini, E., Petraccone S., Perrone, M. G., San- giorgi, G., Lo Porto, C., Lazzati, Z., and Ferrini, B.: Vertical pro- files of particulate matter over Milan during winter 2005/2006, Fresen. Envion. Bull., 16(6), 697–700, 2007.

Ferrero, L., Mocnik, G., Ferrini, B. S., Perrone, M. G., Sangiorgi, G. and Bolzacchini, E.: Vertical profiles of aerosol absorption coefficient from micro-Aethalometer data and Mie calculation over Milan., Sci. Total Environ., 409(14), 2824–37, doi:10.1016/j.scitotenv.2011.04.022, 2011a.

Ferrero, L., Riccio, a., Perrone, M. G., Sangiorgi, G., Ferrini, B. S. and Bolzacchini, E.: Mixing height determination by tethered balloon-based particle soundings and modeling simulations, Atmos. Res, 102(1-2), 145–156, doi:10.1016/j.atmosres.2011.06.016, 2011b.

Ferrero, L., Cappelletti, D., Moroni, B., Sangiorgi, G., Perrone, M. G., Crocchianti, S. and Bolzacchini, E.: Wintertime aerosol dynamics and chemical composition across the mixing layer over basin valleys, Atmos. Environ., 56, 143–153, doi:10.1016/j.atmosenv.2012.03.071, 2012.

Ferrero, L., Castelli, M., Ferrini, B.S., Moscatelli, M., Perrone, M.G., Sangiorgi, G., Rovelli, G., D'Angelo, L., Moroni, B., Scardazza, F., Mocnik, G., Bolzacchini, E., Petitta, M., Cappelletti, D.: Impact of Black Carbon Aerosol over Italian basin valleys: high resolution measurements along vertical profiles, radiative forcing and heating rate. Atmos. Chem. Phys., 14, 9641–9664, 2014.

Fierz, M., Houle, C., Steigmeier, P. and Burtscher, H.: Design, Calibration, and Field Performance of a Miniature Diffusion Size Classifier, Aerosol Science and Technology, 45(1), 1–10, doi:10.1080/02786826.2010.516283, 2011.

Flanner, M. G.: Arctic climate sensitivity to local black carbon, Journal of Geophysical Research: Atmospheres, 118(4), 1840–1851, doi:10.1002/jgrd.50176, 2013.

Francis, J.A., Hunter, E.: New insight into the disappearing Arctic sea ice. EOS Trans. Am. Geophys. Union 87, 509–511, 2006.

Giardi, F., Becagli, S., Traversi, R., Frosini, D., Severi, M., Caiazzo, L., Ancillotti, C., Cappelletti, D., Moroni, B., Grotti, M., Bazzano, A., Lupi, A., Mazzola, M., Vitale, V., Malandrino, M., Ferrero, L., Bolzacchini, E., Viola, A., Udisti, R.: Size distribution and ion composition of aerosol collected at Ny Ålesund in the spring-summer field campaign 2013. Rend. Lincei, *submitted*, 2015.

Granier, C., Niemeier, U., Jungclaus, J. H., Emmons, L., Hess, P., Lamarque, J.-F., Walters, S. and Brasseur, G. P.: Ozone pollution from future ship traffic in the Arctic northern passages, Geophysical Research Letters, 33(13), L13807, doi:10.1029/2006GL026180, 2006.

Guyon, P., Boucher, O., Graham, B., Beck, J., Mayol-Bracero, O. L., Roberts, G. C., Maenhaut, W., Artaxo, P. and Andreae, M. O.: Refractive index of aerosol particles over the Amazon tropical forest during LBA-EUSTACH 1999, J. Aerosol Sci., 34(7), 883–907, doi:10.1016/S0021-8502(03)00052-1, 2003.

Hansen, J., Nazarenko, L.: Soot Climate Forcing via Snow and Ice Albedo. Proc. Natl.Acad. Sci. 101, 423–428. www.pnas.org/doi/10.1073/pnas.2237157100, 2004.

Heim, M., Mullins, B. J., Umhauer, H. and Kasper, G.: Performance evaluation of three optical particle counters with an efficient "multimodal" calibration method, Journal of Aerosol Science, 39(12), 1019–1031, doi:10.1016/j.jaerosci.2008.07.006, 2008.

Heyder, J. and Gebhart, J.: Optimization of response functions of light scattering instruments for size evaluation of aerosol particles, Appl. Optics, 18(5), 705–11, 1979.

Hoffmann, A., Ritter, C., Stock, M., Shiobara, M., Lampert, A., Maturilli, M., Orgis, T. and Neuber, R.: Ground-based lidar measurements from Ny- Alesund during ASTAR, , 9059–9081, 2009.

Howell, S.G., Clarke, A.D., Shinozuka, Y., Kapustin, V., McNaughton, C.S., Huebert, B.J.: Influence of relative humidity upon pollution and dust during ACE-Asia: Size distributions and implications for optical properties, J. Geophys. Res., 111, D06205, doi:10.1029/2004JD005759, 2006.

Intrieri, J.M., Fairall, C.W., Shupe, M.D., Persson, P.O.G., Andreas, E.L., Guest, P.S., Moritz, R.E.: Annual cycle of Arctic surface cloud forcing at SHEBA. J. Geophys. Res., 107 (C10), doi:10.1029/2000JC000439, 2002.

IPCC, 2013: Climate Change 2013: The Physical Science Basis. Cambridge University Press, Cambridge, United Kingdom and New York, USA, 2013.

Jacobson, M.Z.: Short-term effects of controlling fossil-fuel soot, biofuel soot and gases, and methane on climate, arctic ice, and air pollution health, J. Geophys. Res., 115, D14209, doi:10.1029/2009JD013795, 2010.

Kaufman, Y.J., Tanré, D., Boucher, O.: A satellite view of aerosols in the climate system. Nature, 419, 215-223, 2002.

Kirkby, J., Curtius, J., Almeida, J., Dunne, E., Duplissy, J., Ehrhart, S., Franchin, A., Gagné, S., Ickes, L., Kürten, A., Kupc, A., Metzger, A., Riccobono, F., Rondo, L., Schobesberger, S., Tsagkogeorgas, G., Wimmer, D., Amorim, A., Bianchi, F., Breitenlechner, M., David, A., Dommen, J., Downard, A., Ehn, M., Flagan, R. C., Haider, S., Hansel, A., Hauser, D., Jud, W., Junninen, H., Kreissl, F., Kvashin, A., Laaksonen, A., Lehtipalo, K., Lima, J., Lovejoy, E. R., Makhmutov, V., Mathot, S., Mikkilä, J., Minginette, P., Mogo, S., Nieminen, T., Onnela, A., Pereira, P., Petäjä, T., Schnitzhofer, R., Seinfeld, J. H., Sipilä, M., Stozhkov, Y., Stratmann, F., Tomé, A., Vanhanen, J., Viisanen, Y., Vrtala, A., Wagner, P. E., Walther, H., Weingartner, E., Wex, H., Winkler, P. M., Carslaw, K. S., Worsnop, D. R., Baltensperger, U. and Kulmala, M.: Role of sulphuric acid, ammonia and galactic cosmic rays in atmospheric aerosol nucleation., Nature, 476(7361), 429–33, doi:10.1038/nature10343, 2011.

Koch, D., Schulz, M., Kinne, S., Mcnaughton, C., Spackman, J. R., Balkanski, Y., Bauer, S. and Berntsen, T.: and Physics Evaluation of black carbon estimations in global aerosol models, , (November), 9001–9026, 2009.

Koren, I., Kaufman, Y.J., Remer, L.A., Martins, J.V.: Measurments of the effect of amazon smoke on inhibition of cloud formation. Scienze, 303, 1342-1345, 2004.

Koren, I., Martins, J.V., Remer, L.A., Afargan, H.: Smoke invigoration versus inhibition of clouds over the amazon, Science, 321, 946-949, 2008.

Kupiszewski, P., Leck, C., Tjernström, M., Sjogren, S., Sedlar, J., Graus, M., Müller, M., Brooks, B., Swietlicki, E., Norris, S. and Hansel, a.: Vertical profiling of aerosol particles and trace gases over the central Arctic Ocean

during summer, Atmospheric Chemistry and Physics, 13(24), 12405–12431, doi:10.5194/acp-13-12405-2013, 2013.

Lanconelli, C., Busetto, M., Mazzola, M., Lupi, A., Becagli, S., Frosini, D., Virkkula, A., Vitale, V.: Physical, Chemical and Optical Properties of Aerosol at Ny Ålesund, 189 Svalbard: a Closure Study. Proceeding at the 1st Iberian Meeting on Aerosol Science and Technology, July 1-3, 2013, ISBN: 978-989-20-3962-6, pages 189-192, 2013.

Lawson, R. P., Stamnes, K., Stamnes, J., Zmarzly, P., Koskuliks, J., Roden, C., Mo, Q., Carrithers, M. and Bland, G. L.: Deployment of a Tethered-Balloon System for Microphysics and Radiative Measurements in Mixed-Phase Clouds at Ny-Ålesund and South Pole, Journal of Atmospheric and Oceanic Technology, 28(5), 656–670, doi:10.1175/2010JTECHA1439.1, 2011.

Liu, Y. and Daum, P. H.: Relationship of refractive index to mass density and self-consistency of mixing rules for multicomponent mixtures like ambient aerosols, J. Aerosol Sci., 39(11), 974–986, doi:10.1016/j.jaerosci.2008.06.006, 2008.

Lovejoy, E. R.: Atmospheric ion-induced nucleation of sulfuric acid and water, Journal of Geophysical Research, 109(D8), D08204, doi:10.1029/2003JD004460, 2004.

Ma, X., Lu, J. Q., Brock, R. S., Jacobs, K. M., Yang, P. and Hu, X.-H.: Determination of complex refractive index of polystyrene microspheres from 370 to 1610 nm., Physics in medicine and biology, 48(24), 4165–72 [online] Available from: http://www.ncbi.nlm.nih.gov/pubmed/14727759, 2003.

Manabe, S., Wetherald, R.T.: The effect of doubling the CO_2 concentration on the climate of a general circulation model. J. Atmos. Sci. 32, 3–15, 1975.

Mazzola M., Viola A.P., Lanconelli C., and Vitale V: Atmospheric observations at the Amundsen-Nobile Climate Change Tower in Ny-Alesund, Svalbard. Rend. Lincei, *submitted*, 2015a.

Mazzola, M., Tampieri, F., Viola, A.P., Lanconelli, C. and Choi, T.: Stable boundary layer vertical scales in the Arctic: observations and analyses at Ny-Ålesund, Svalbard. Quarterly Journal of the Royal Meteorological Society, *in press*, doi: 10.1002/qj.2727, 2015b.

Moroni, B., Becagli, S., Bolzacchini, E., Busetto, M., Cappelletti, D., Crocchianti, S., Ferrero, L., Frosini, D., Lanconelli, C., Lupi, A., Maturilli, M., Mazzola, M., Perrone, G., Sangiorgi, G., Traversi, R., Udisti, R., Viola A., Vitale, V.: Sources and properties of aerosol particles upon Ny-Ålesund (Svalbard Islands): results of integrated vertical profile measurements and electron microscopy analyses. Advances in Meteorology, 2015, 292081, 1-11, 2015.

Nozaki, Y.: A Fresh Look at Element Distribution in the North Pacific. http://www.agu.org/eos_elec/97025e.html, 1997.

Ødemark, K., Dalsøren, S. B., Samset, B. H., Berntsen, T. K., Fuglestvedt, J. S. and Myhre, G.: Short-lived climate forcers from current shipping and petroleum activities in the Arctic, Atmospheric Chemistry and Physics, 12(4), 1979–1993, doi:10.5194/acp-12-1979-2012, 2012.

Overland, J.E., Wang, M.: Large-scale atmospheric circulation changes are associated with the recent loss of Arctic sea ice. Tellus 62A, 1–9, 2010.

Quinn, P. K., Bates, T. S., Baum, E., Doubleday, N., Fiore, a. M., Flanner, M., Fridlind, a., Garrett, T. J., Koch, D., Menon, S., Shindell, D., Stohl, a. and Warren, S. G.: Short-lived pollutants in the Arctic: their climate impact and possible mitigation strategies, Atmospheric Chemistry and Physics, 8(6), 1723–1735, doi:10.5194/acp-8-

1723-2008, 2008.

Ramana, M. V, Ramanathan, V., Kim, D., Roberts, G. C. and Corrigan, C. E.: Albedo , atmospheric solar absorption and heating rate measurements with stacked UAVs, , 1931, 1913–1931, doi:10.1002/qj, 2007.

Ramanathan, V. and Feng, Y.: Air pollution, greenhouse gases and climate change: Global and regional perspectives, Atmos. Environ., 43(1), 37–50, doi:10.1016/j.atmosenv.2008.09.063, 2009.

Reche, C., Querol, X., Alastuey, A., Viana, M., Pey, J., Moreno, T., Rodríguez, S., González, Y., Fernández-Camacho, R., de la Rosa, J., Dall'Osto, M., Prévôt, A. S. H., Hueglin, C., Harrison, R. M. and Quincey, P.: New considerations for PM, Black Carbon and particle number concentration for air quality monitoring across different European cities, Atmospheric Chemistry and Physics, 11(13), 6207–6227, doi:10.5194/acp-11-6207-2011, 2011.

Reddington, C. L., Carslaw, K. S., Spracklen, D. V., Frontoso, M. G., Collins, L., Merikanto, J., Minikin, a., Hamburger, T., Coe, H., Kulmala, M., Aalto, P., Flentje, H., Plass-Dülmer, C., Birmili, W., Wiedensohler, a., Wehner, B., Tuch, T., Sonntag, a., O'Dowd, C. D., Jennings, S. G., Dupuy, R., Baltensperger, U., Weingartner, E., Hansson, H. C., Tunved, P., Laj, P., Sellegri, K., Boulon, J., Putaud, J. P., Gruening, C., Swietlicki, E., Roldin, P., Henzing, J. S., Moerman, M., Mihalopoulos, N., Kouvarakis, G., Ždímal, V., Zíková, N., Marinoni, a., Bonasoni, P. and Duchi, R.: Primary versus secondary contributions to particle number concentrations in the European boundary layer, Atmospheric Chemistry and Physics, 11(23), 12007–12036, doi:10.5194/acp-11-12007-2011, 2011.

Riccobono, F., Schobesberger, S., Scott, C. E., Dommen, J., Ortega, I. K., Rondo, L., Almeida, J., Amorim, A., Bianchi, F., Breitenlechner, M., David, A., Downard, A., Dunne, E. M., Duplissy, J., Ehrhart, S., Flagan, R. C., Franchin, A., Hansel, A., Junninen, H., Kajos, M., Keskinen, H., Kupc, A., Kurten, A., Kvashin, A. N., Laaksonen, A., Lehtipalo, K., Makhmutov, V., Mathot, S., Nieminen, T., Onnela, A., Petaja, T., Praplan, A. P., Santos, F. D., Schallhart, S., Seinfeld, J. H., Sipila, M., Spracklen, D. V., Stozhkov, Y., Stratmann, F., Tome, A., Tsagkogeorgas, G., Vaattovaara, P., Viisanen, Y., Vrtala, A., Wagner, P. E., Weingartner, E., Wex, H., Wimmer, D., Carslaw, K. S., Curtius, J., Donahue, N. M., Kirkby, J., Kulmala, M., Worsnop, D. R. and Baltensperger, U.: (Suppl.) Oxidation Products of Biogenic Emissions Contribute to Nucleation of Atmospheric Particles, Science, 344(6185), 717–721, doi:10.1126/science.1243527, 2014.

Rodrıguez, S. and Cuevas, E.: The contributions of "minimum pri- mary emissions" and "new particle formation enhancements" to the particle number concentration in urban air, J. Aerosol Sci., 38, 1207–1219, doi:10.1016/j.jaerosci.2007.09.001, 2007.

Samset, B. H., Myhre, G., Schulz, M., Balkanski, Y., Bauer, S., Berntsen, T. K., Bian, H., Bellouin, N., Diehl, T., Easter, R. C., Ghan, S. J., Iversen, T., Kinne, S., Kirkevåg, a., Lamarque, J.-F., Lin, G., Liu, X., Penner, J. E., Seland, Ø., Skeie, R. B., Stier, P., Takemura, T., Tsigaridis, K. and Zhang, K.: Black carbon vertical profiles strongly affect its radiative forcing uncertainty, Atmospheric Chemistry and Physics, 13(5), 2423–2434, doi:10.5194/acp-13-2423-2013, 2013.

Samset, B. H., Myhre, G., Herber, a., Kondo, Y., Li, S.-M., Moteki, N., Koike, M., Oshima, N., Schwarz, J. P., Balkanski, Y., Bauer, S. E., Bellouin, N., Berntsen, T. K., Bian, H., Chin, M., Diehl, T., Easter, R. C., Ghan, S. J., Iversen, T., Kirkevåg, a., Lamarque, J.-F., Lin, G., Liu, X., Penner, J. E., Schulz, M., Seland, Ø., Skeie, R. B., Stier, P., Takemura, T., Tsigaridis, K. and Zhang, K.: Modeled black carbon radiative forcing and atmospheric lifetime in AeroCom Phase II constrained by aircraft observations., 2014a.

Samset, B. H., Myhre, G., Herber, a., Kondo, Y., Li, S.-M., Moteki, N., Koike, M., Oshima, N., Schwarz, J. P.,

Balkanski, Y., Bauer, S. E., Bellouin, N., Berntsen, T. K., Bian, H., Chin, M., Diehl, T., Easter, R. C., Ghan, S. J., Iversen, T., Kirkevåg, a., Lamarque, J.-F., Lin, G., Liu, X., Penner, J. E., Schulz, M., Seland, Ø., Skeie, R. B., Stier, P., Takemura, T., Tsigaridis, K. and Zhang, K.: Modelled black carbon radiative forcing and atmospheric lifetime in AeroCom Phase II constrained by aircraft observations, Atmospheric Chemistry and Physics, 14(22), 12465–12477, doi:10.5194/acp-14-12465-2014, 2014b.

Sangiorgi, G., Ferrero, L., Perrone, M. G., Bolzacchini, E., Duane, M. and Larsen, B. R.: Vertical distribution of hydrocarbons in the low troposphere below and above the mixing height : Tethered balloon measurements in Milan, Italy, Environ. Pollut., 159(12), 3545–3552, doi:10.1016/j.envpol.2011.08.012, 2011.

Sand, M., Berntsen, T. K., Kay, J. E., Lamarque, J. F., Seland, Ø. and Kirkevåg, a.: The Arctic response to remote and local forcing of black carbon, Atmospheric Chemistry and Physics, 13(1), 211–224, doi:10.5194/acp-13-211-2013, 2013.

Schmid, O., Artaxo, P., Arnott, W. P., Chand, D., Gatti, L. V., Frank, G. P., Hoffer, a., Schnaiter, M. and Andreae, M. O.: Spectral light absorption by ambient aerosols influenced by biomass burning in the Amazon Basin. I: Comparison and field calibration of absorption measurement techniques, Atmospheric Chemistry and Physics, 6(11), 3443–3462, doi:10.5194/acp-6-3443-2006, 2006.

Schmid, O., Artaxo, P., Arnott, W. P., Chand, D., Gatti, L. V., Frank, G. P., Hoffer, a., Schnaiter, M. and Andreae, M. O.: Spectral light absorption by ambient aerosols influenced by biomass burning in the Amazon Basin. I: Comparison and field calibration of absorption measurement techniques, Atmos. Chem. Phys., 6(11), 3443–3462, doi:10.5194/acp-6-3443-2006, 2006.

Schumann, T.: On the use of a modified clean-room optical particle counter for atmosperic aerosols at high relative humidity, Atmospheric Research, 25(6), 499–520, doi:10.1016/0169-8095(90)90035-B, 1990.

Schwarz, J. P., Spackman, J. R., Gao, R. S., Watts, L. a., Stier, P., Schulz, M., Davis, S. M., Wofsy, S. C. and Fahey, D. W.: Global-scale black carbon profiles observed in the remote atmosphere and compared to models, Geophysical Research Letters, 37(18), n/a–n/a, doi:10.1029/2010GL044372, 2010.

Screen, J.A., Simmonds, I.: The central role of diminishing sea ice in recent Arctic temperature amplification. Nature 464, 1334–1337, 2010a.

Screen, J.A., Simmonds, I.: Increasing fall-winter energy loss from the Arctic Ocean and its role in Arctic temperature amplification. Geophys. Res. Lett. 37, L16707. doi:10.1029/2010GL044136, 2010b.

Seibert, P., Beyrich, F., Gryning, S., Jo, S., Rasmussen, A. and Tercier, P.: Review and intercomparison of operational methods for the determination of the mixing height,Atmospheric Environment, 34, 1001–1027,doi:10.1016/S1352-2310(99)00349-0 2000.

Seinfeld, J.H., Pandis, S.N.; Atmos. Chem. Phys. – From air pollution to climate change. Wiley-Interscience edition, 2006.

Serreze, M. C. and Barry, R. G.: Processes and impacts of Arctic amplification: A research synthesis, Global and Planetary Change, 77(1-2), 85–96, doi:10.1016/j.gloplacha.2011.03.004, 2011.

Serreze, M. C., Barrett, A. P., Slater, A. G., Steele, M., Zhang, J. and Trenberth, K. E.: The large-scale energy budget of the Arctic, Journal of Geophysical Research, 112(D11), D11122, doi:10.1029/2006JD008230, 2007.

Shindell, D. and Faluvegi, G.: Climate response to regional radiative forcing during the twentieth century, Nature Geoscience, 2(4), 294–300, doi:10.1038/ngeo473, 2009.

Shindell, D., Kuylenstierna, J.C.I., Vignati, E., Van Dingenen, R., Amann, M., Klimont, Z., Anenberg, S.C., Muller, N., et al.: Simultaneously mitigating near-term climate change and improving human health and food security, Science, 335 (6065), 183–189, doi:10.1126/science.1210026, 2012.

Spackman, J. R., Gao, R. S., Neff, W. D., Schwarz, J. P., Watts, L. a., Fahey, D. W., Holloway, J. S., Ryerson, T. B., Peischl, J. and Brock, C. a.: Aircraft observations of enhancement and depletion of black carbon mass in the springtime Arctic, Atmospheric Chemistry and Physics, 10(19), 9667–9680, doi:10.5194/acp-10-9667-2010, 2010.

Stock, M., Ritter, C., Herber, a., von Hoyningen-Huene, W., Baibakov, K., Gräser, J., Orgis, T., Treffeisen, R., Zinoviev, N., Makshtas, a. and Dethloff, K.: Springtime Arctic aerosol: Smoke versus haze, a case study for March 2008, Atmospheric Environment, 52(March 2008), 48–55, doi:10.1016/j.atmosenv.2011.06.051, 2012.

Ström, J., Umegård, J., Tørseth, K., Tunved, P., Hansson, H.-C., Holmén, K., Wismann, V., Herber, a. and König-Langlo, G.: One year of particle size distribution and aerosol chemical composition measurements at the Zeppelin Station, Svalbard, March 2000–March 2001, Physics and Chemistry of the Earth, Parts A/B/C, 28(28-32), 1181–1190, doi:10.1016/j.pce.2003.08.058, 2003.

Ström, J., Engvall, A.-C., Delbart, F., Krejci, R. and Treffeisen, R.: On small particles in the Arctic summer boundary layer: observations at two different heights near Ny-Ålesund, Svalbard, Tellus B, 61(2), 473–482, doi:10.1111/j.1600-0889.2008.00412.x, 2009.

Tunved, P., Ström, J. and Krejci, R.: Arctic aerosol life cycle: linking aerosol size distributions observed between 2000 and 2010 with air mass transport and precipitation at Zeppelin station, Ny-Ålesund, Svalbard, Atmospheric Chemistry and Physics, 13(7), 3643–3660, doi:10.5194/acp-13-3643-2013, 2013.

Turpin, B.J., Lim, H.J.: Species contributions to PM2.5 mass concentrations: revisiting common assumptions for estimating organic mass. Aerosol Sci Technol., 35, 602–10, 2001.

Udisti, R., Becagli, S., Benassai, S., Castellano, E., Fattori, I., Innocenti, M., Migliori, A., Traversi, R.:Atmosphere-snow interaction by a comparison between aerosol and uppermost snow layers composition at Dome C (East Antarctica). Ann. Glaciol., 39, 53-61, 2004.

Udisti, R., Dayan, U., Becagli, S., Busetto, M., Frosini, D., Legrand, M., Lucarelli, F., Preunkert, S., Severi, M., Traversi, R., Vitale, V.:Sea-spray aerosol in central Antarctica. Present atmospheric behavior and implications for paleoclimatic reconstructions. Atmos. Environ., 52, 109-120, 2012.

Udisti, R., Becagli, S., Frosini, D., Ghedini, C., Rugi, F., Severi, M., Traversi, R., Zanini, R., Calzolai, G., Chiari, M., Lucarelli, F., Nava, S., Ardini F, Grotti M, Vione D, Malandrino M, Bolzacchini E, Ferrero, L., Perrone, M.G., Sangiorgi, G., Francesconi, S., Giannarelli, S., Cappelletti, D., Moroni, B., Ceccato, D., Mittner, P., Sartori, P.: Activity and preliminary results from the 2011-2012 field seasons at Ny-Ålesund. vol. DTA 14/2013, p. 53-68, CNR Edizioni, ISSN 2239-5172, 2013.

Udisti, R., Bazzano, A., Becagli, S., Bolzacchini, E., Caiazzo, L., Cappelletti, D., Ferrero, L., Frosini, D., Giardi, F., Grotti, M., Lupi, A., Malandrino, M., Mazzola, M., Moroni, B., Severi, M., Traversi, R., Viola, A., Vitale, V.: Sulfate source apportionment in the Ny Ålesund (Svalbard Islands) Arctic aerosol. Rend. Lincei, *submitted*, 2015.

Vavrus, S., Waliser, D., Schweiger, A., Francis, J.A.: Simulations of 20th and 21st century Arctic cloud amount in the global climate models assessed in the IPCC AR4. Climate Dyn. 33, 1099–1115. doi:10.1007/s00382-008-0475-6, 2009.

Viola, A., Vitale, V., Petroni, I., Tampieri, F., Mazzola, M., Lanconelli, C., Busetto, M., Lupi, A., Di Liberto, L., Conidi, A., Ianniello, A., Salvatori, R., Esposito, G., Spataro., F., Udisti, R., Becagli, S., Frosini, D., Ghedini, C., Traversi, R., Cappelletti, D., Valt, M., Turetta, C.: Atmospheric studies at "Dirigibile Italia". vol. DTA 14/2013, p. 35-52, CNR Edizioni, ISSN 2239-5172, 2013.

Wagenbach, D., Preunkert, S., Schäfer, J., Jung, W., and Tomadin, L.: Northward transport of Saharan dust recorded in a deep alpine ice core, in: The Impact of Desert Dust Across the Mediterranean, edited by: Guerzoni, S. and Chester, R., Environmental Science and Technology Library, vol. 11, Springer, the Netherlands, 291–300, 1996.

Weingartner, E., Saathoff, H., Schnaiter, M., Streit, N., Bitnar, B. and Baltensperger, U.: Absorption of light by soot particles: determination of the absorption coefficient by means of aethalometers, J. Aerosol Sci., 34(10), 1445–1463, doi:10.1016/S0021-8502(03)00359-8, 2003.

Yang, X.-Y., Fyfe, J.C., Flato, G.M.: The role of poleward energy transport in Arctictemperature evolution. Geophys. Res. Lett. 37, L14803. doi:10.1029/2010GL042487, 2010.

Zangrando, R., Barbaro, E., Zennaro, P., Rossi, S., Kehrwald, N. M., Gabrieli, J., Barbante, C. and Gambaro, A.: Molecular markers of biomass burning in Arctic aerosols, Environmental Science and Technology, 47(15), 8565–8574, doi:10.1021/es400125r, 2013.

Atmos. Chem. Phys. Discuss., doi:10.5194/acp-2016-171, 2016
Manuscript under review for journal Atmos. Chem. Phys.
Published: 13 April 2016

Atmospheric Chemistry and Physics Discussions

Date	UTC Time	N° profiles	max altitude (m)	Cloud base (m)
Spring 2011				
30-03-2011	1240-1518	6	741	No clouds
01-04-2011	0630-1725	10	788	No clouds
04-04-2011	1817-2018	6	748	1152
06-04-2011	1642-1922	8	716	No clouds
07-04-2011	1251-1923	10	712	No clouds
08-04-2011	0825-1944	14	740	No clouds/1534[(1)]
10-04-2011	1245-1438	6	300	No clouds/984[(2)]
14-04-2011	1502-1558	5	738	No clouds
22-04-2011	1917-2009	4	846	No clouds
23-04-2011	1210-1334	6	1008	2414
26-04-2011	1607-2200	8	1152	No clouds
30-04-2011	0946-1048	6	855	4018
Summer 2011				
06-07-2011	0740-1755	10	1143	No clouds/2813[(3)]
08-07-2011	1643-2053	2	1208	1787
12-07-2011	0819-1001	6	724	506
Summer 2012				
21-06-2012	1512-1611	2	980	No clouds
23-06-2012	0555-1107	12	1024	622
24-06-2012	1102-1516	8	1076	No clouds
26-06-2012	0743-1300	10	948	No clouds
29-06-2012	0758-1319	10	1144	No clouds
30-06-2012	0920-2030	8	1100	No clouds/821[(4)]
01-07-2012	0835-2140	10	1212	No clouds
04-07-2012	1330-1805	8	1192	654
10-07-2012	0844-2107	8	1268	No clouds
11-07-2012	0837-2320	14	1196	No clouds/722[(5)]

Table 1. Dates, UTC time, number of profiles, maximum altitude and sky conditions reached during the 2011-2012 Spring-Summer campaign in Ny-Ålesund; [(1)]from 1600 UTC (last 6 profiles), [(2)]variable for half of the time, [(3)]variable for half of the time, [(4)]clouds until 1130 UTC, [(5)]from 2219 UTC (last 2 profiles).

5

Atmos. Chem. Phys. Discuss., doi:10.5194/acp-2016-171, 2016
Manuscript under review for journal Atmos. Chem. Phys.
Published: 13 April 2016

Atmospheric Chemistry and Physics Discussions

Season	Profile Type		T (°C)				RH (%)				WS (m/s)				P (hPa)
			33 m	10 m	5 m	2 m	33 m	10 m	5 m	2 m	33 m	10 m	5 m	2 m	Ground
Spring	HO	mean	-8.5	-8.9	-9.7	-9.7	61.0	61.2	61.8	62.7	0.6	0.7	0.6	0.6	997.4
		σ_m	0.5	0.5	0.5	0.5	1.0	1.0	0.9	0.9	0.1	0.1	0.1	0.1	0.4
	PG	mean	-4.7	-5.2	-5.8	-5.9	64.8	65.0	65.9	67.3	2.3	2.1	1.8	1.7	996.2
		σ_m	0.2	0.3	0.3	0.3	0.4	0.4	0.4	0.4	0.1	0.1	0.1	0.1	0.5
	NG	mean	-8.9	-9.3	-9.9	-9.9	57.2	58.5	59.1	60.1	1.3	1.1	1.0	0.9	992.8
		σ_m	0.2	0.2	0.2	0.2	0.4	0.3	0.3	0.3	0.1	0.1	0.1	0.1	0.2
	DNG	mean	-15.8	-16.5	-17.2	-17.2	72.6	73.2	72.9	73.6	0.7	0.9	1.0	0.9	994.8
		σ_m	0.3	0.3	0.3	0.3	0.5	0.3	0.3	0.3	0.1	0.1	0.1	0.1	0.4
Summer	HO	mean	5.7	5.8	5.5	6.0	76.5	75.3	74.7	74.9	4.1	3.8	3.6	3.4	1004.1
		σ_m	0.1	0.1	0.1	0.1	0.2	0.2	0.2	0.2	0.1	0.1	0.1	0.1	0.2
	SP	mean	5.8	5.9	5.6	6.1	78.0	76.4	75.6	75.8	2.6	2.6	2.5	2.4	1001.9
		σ_m	0.1	0.1	0.1	0.1	0.2	0.2	0.2	0.2	0.1	0.1	0.1	0.1	0.1

Table 2. Meteorological parameters (temperature, relative humidity, wind speed, pressure) measured at the CCT at different levels (33, 20, 5 and 2 m) and averaged (timely coincident) for each profile class.

Atmos. Chem. Phys. Discuss., doi:10.5194/acp-2016-171, 2016
Manuscript under review for journal Atmos. Chem. Phys.
Published: 13 April 2016

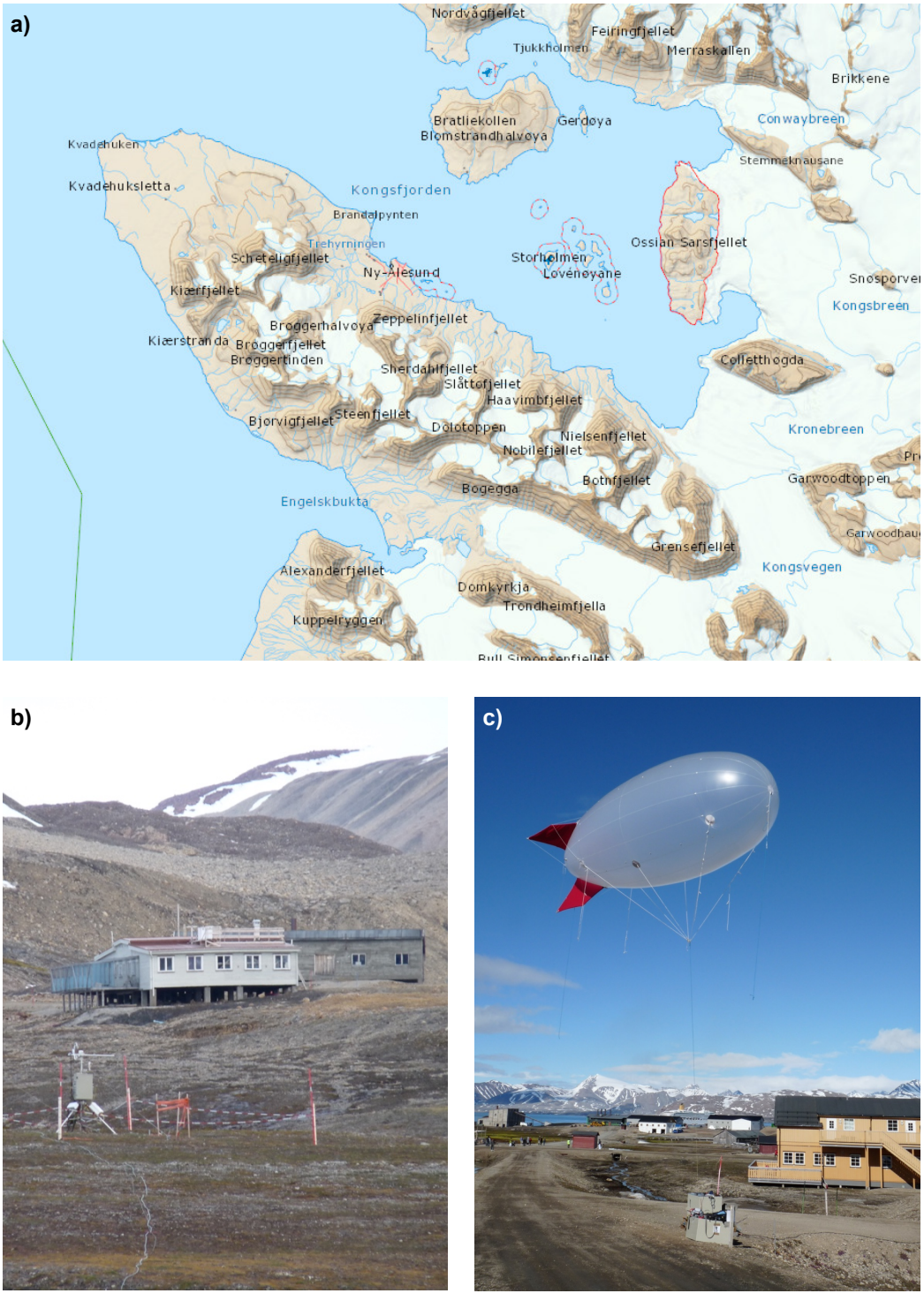

Figure 1. a) Ny-Ålesund, the Kongsfjord and the surrounding orography; b) Gruvebadet sampling site; c) the tethered balloon in Ny-Ålesund.

Atmos. Chem. Phys. Discuss., doi:10.5194/acp-2016-171, 2016
Manuscript under review for journal Atmos. Chem. Phys.
Published: 13 April 2016

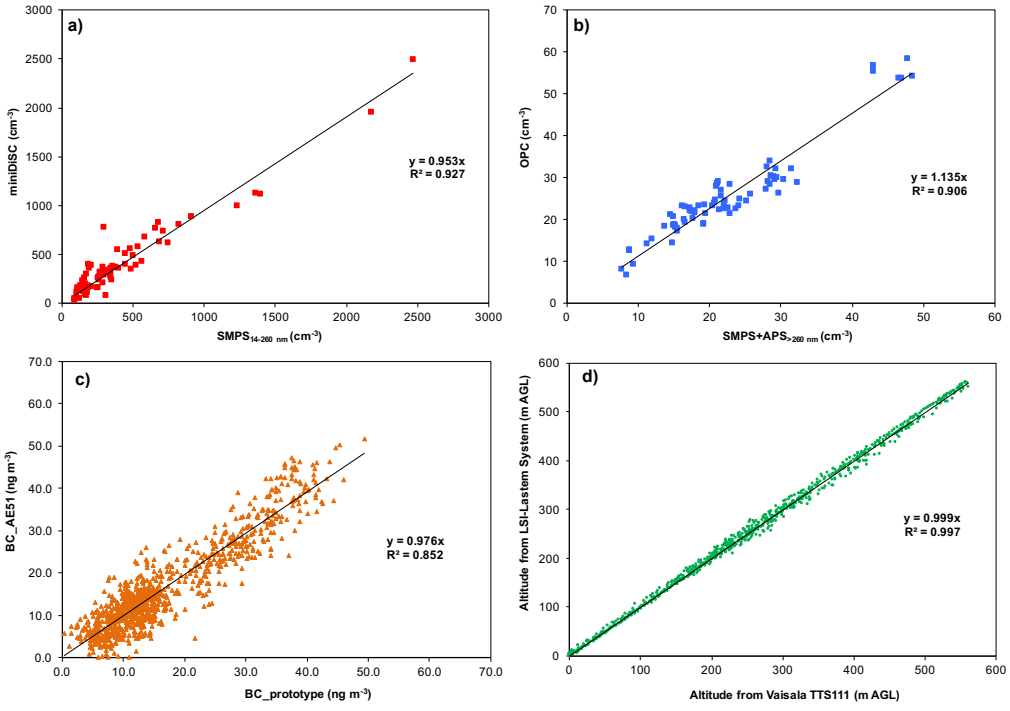

Figure 2. Linear correlations between: a) $N_{14\text{-}260}$ measured with the miniDiSC and with the SMPS; b) $N_{>260}$measured with the OPC and with the SMPS+APS; c) BC measured with AE51 and the micro-Atehalometer prototype; d) altitude obtained with the LSI-Lastem meteorological station and with the Vaisala tethersonde.

Atmos. Chem. Phys. Discuss., doi:10.5194/acp-2016-171, 2016
Manuscript under review for journal Atmos. Chem. Phys.
Published: 13 April 2016

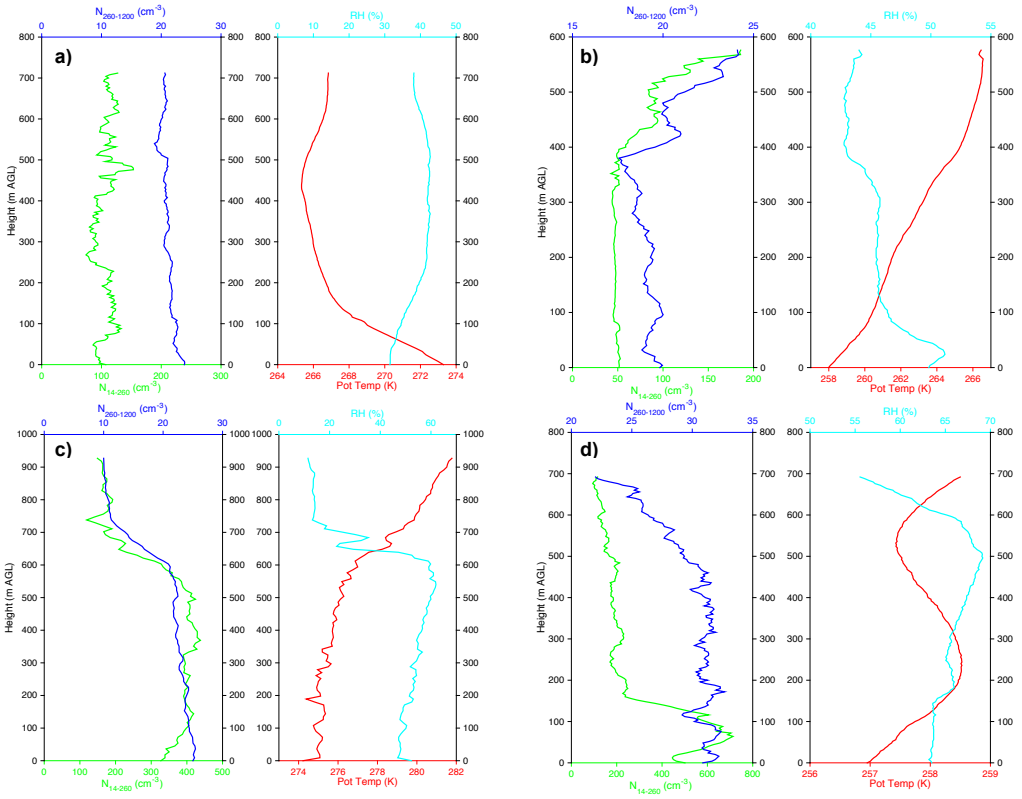

Figure 3. Vertical profiles of $N_{14\text{-}260}$ (green line), $N_{260\text{-}1200}$ (blue line), potential temperature (red line) and relative humidity (light blue line) measured over Ny-Ålesund on: a) 7th April 2011 (1251-1310 UTC); b) 1st April 2011 (0630-0657 UTC); c) 23th April 2011 (1321-1334 UTC); d) 6th April 2011 (1803-1822 UTC).

Atmos. Chem. Phys. Discuss., doi:10.5194/acp-2016-171, 2016
Manuscript under review for journal Atmos. Chem. Phys.
Published: 13 April 2016

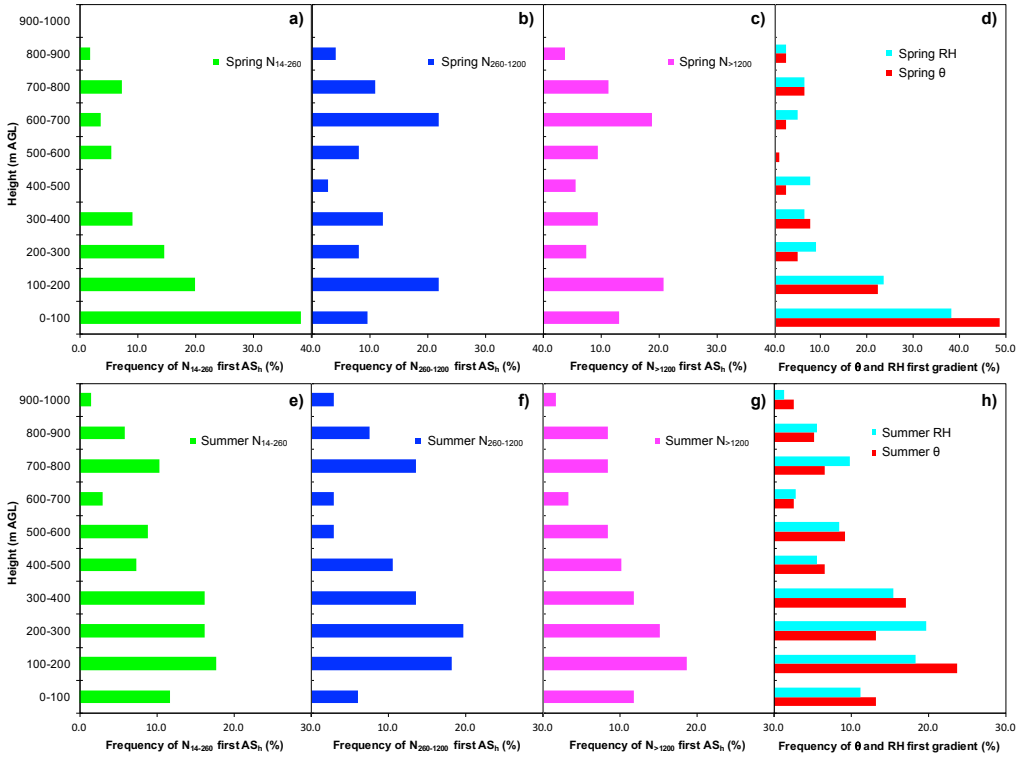

Figure 4. Vertical frequency distribution of the AS_h for N_{14-260}, $N_{260-1200}$, $N_{>1200}$, θ and RH during spring in panels from a) to d) and in summer in panels from e) to h).

Atmos. Chem. Phys. Discuss., doi:10.5194/acp-2016-171, 2016
Manuscript under review for journal Atmos. Chem. Phys.
Published: 13 April 2016

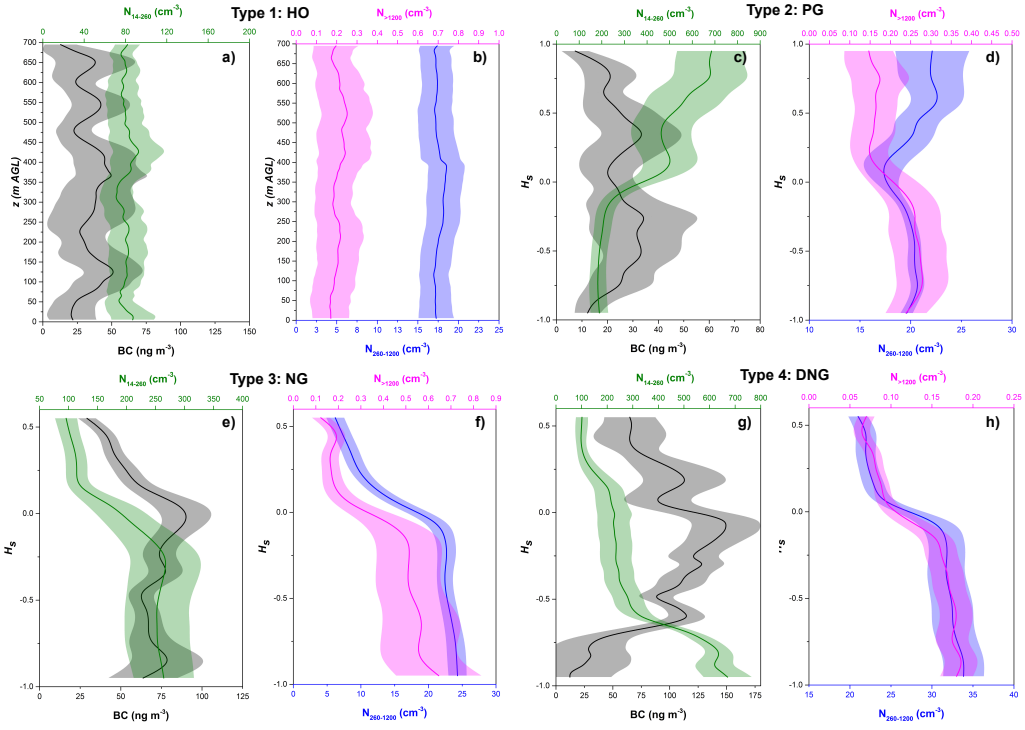

Figure 5. Springtime statistical mean profiles of $N_{14\text{-}260}$ (green line), BC (black line), $N_{260\text{-}1200}$ (blue line) and $N_{>1200}$ (magenta line) along standardized height H_s over Ny- Ålesund for the four typologies of vertical profiles: a-b) homogeneous profiles (HO); c-d) positive gradient profiles (PG); e-f) negative gradient profiles (NG); g-h) decoupled negative gradient profiles (DNG).

Atmos. Chem. Phys. Discuss., doi:10.5194/acp-2016-171, 2016
Manuscript under review for journal Atmos. Chem. Phys.
Published: 13 April 2016

Atmospheric Chemistry and Physics Discussions

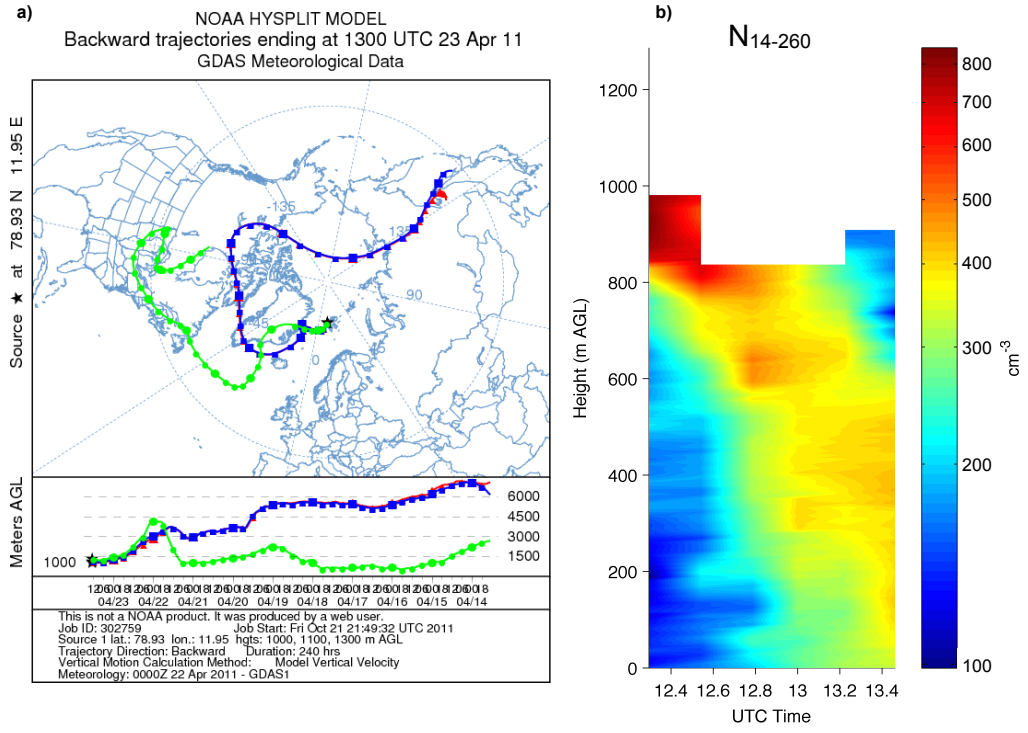

Figure 6. Case study of 23th April 2011 (1200-1330 UTC): a) air mass backtrajectories; b) time evolution of $N_{14\text{-}260}$ obtained through the interpolation of 6 vertical profiles, each of which lasted ~15 min and was distanced ~1 min from the following profile.

Atmos. Chem. Phys. Discuss., doi:10.5194/acp-2016-171, 2016
Manuscript under review for journal Atmos. Chem. Phys.
Published: 13 April 2016

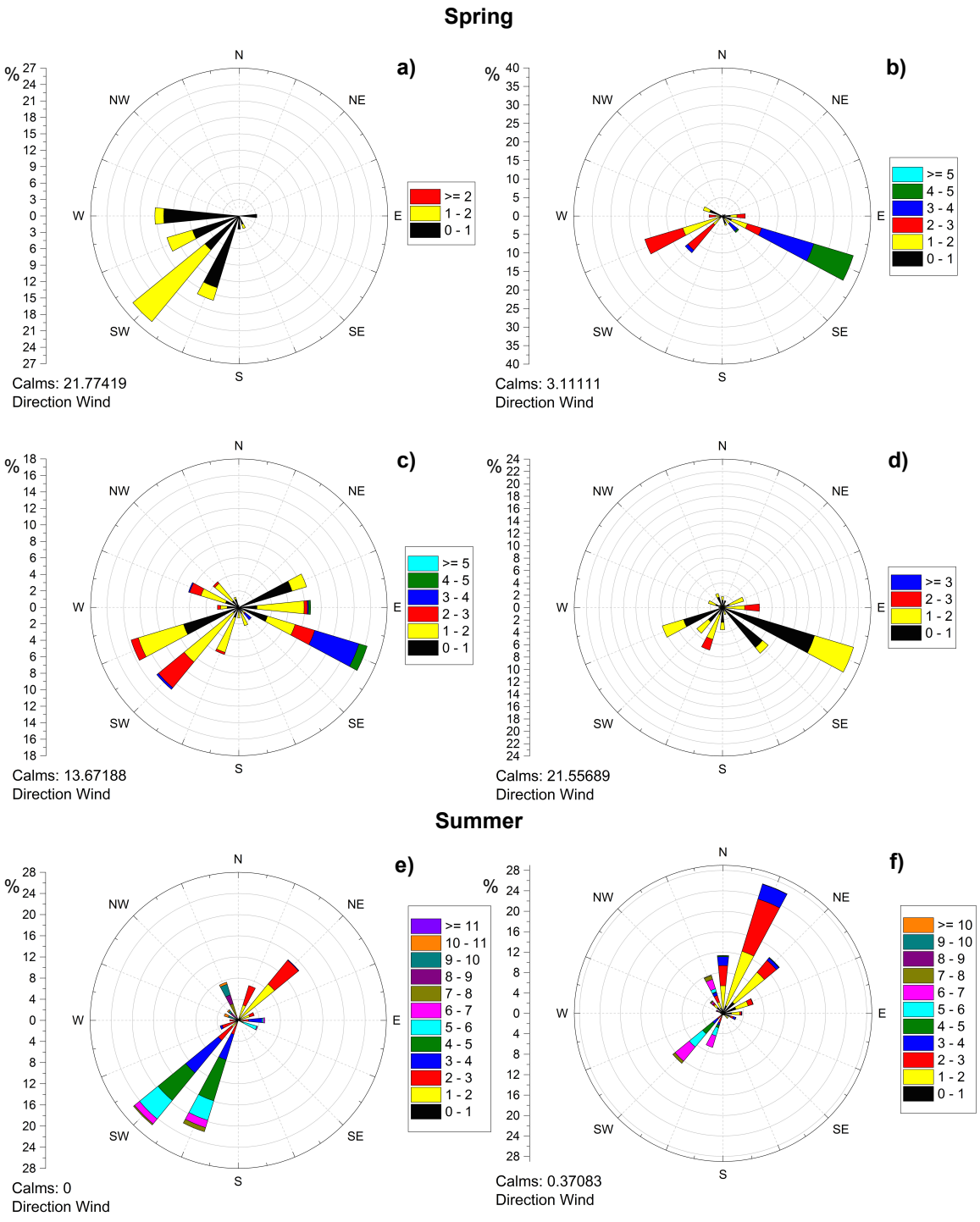

Figure 7. Wind rose obtained from the measured wind speed and direction at the CCT (33 m). Springtime wind rose timely coincident with: a) homogeneous profiles (HO); b) positive gradient profiles (PG); c) negative gradient profiles (NG); d) decoupled negative gradient profiles (DNG). Summertime wind rose timely coincident with: e) homogeneous profiles (HO); f) profiles impacted by shipping emissions (SP).

Atmos. Chem. Phys. Discuss., doi:10.5194/acp-2016-171, 2016
Manuscript under review for journal Atmos. Chem. Phys.
Published: 13 April 2016

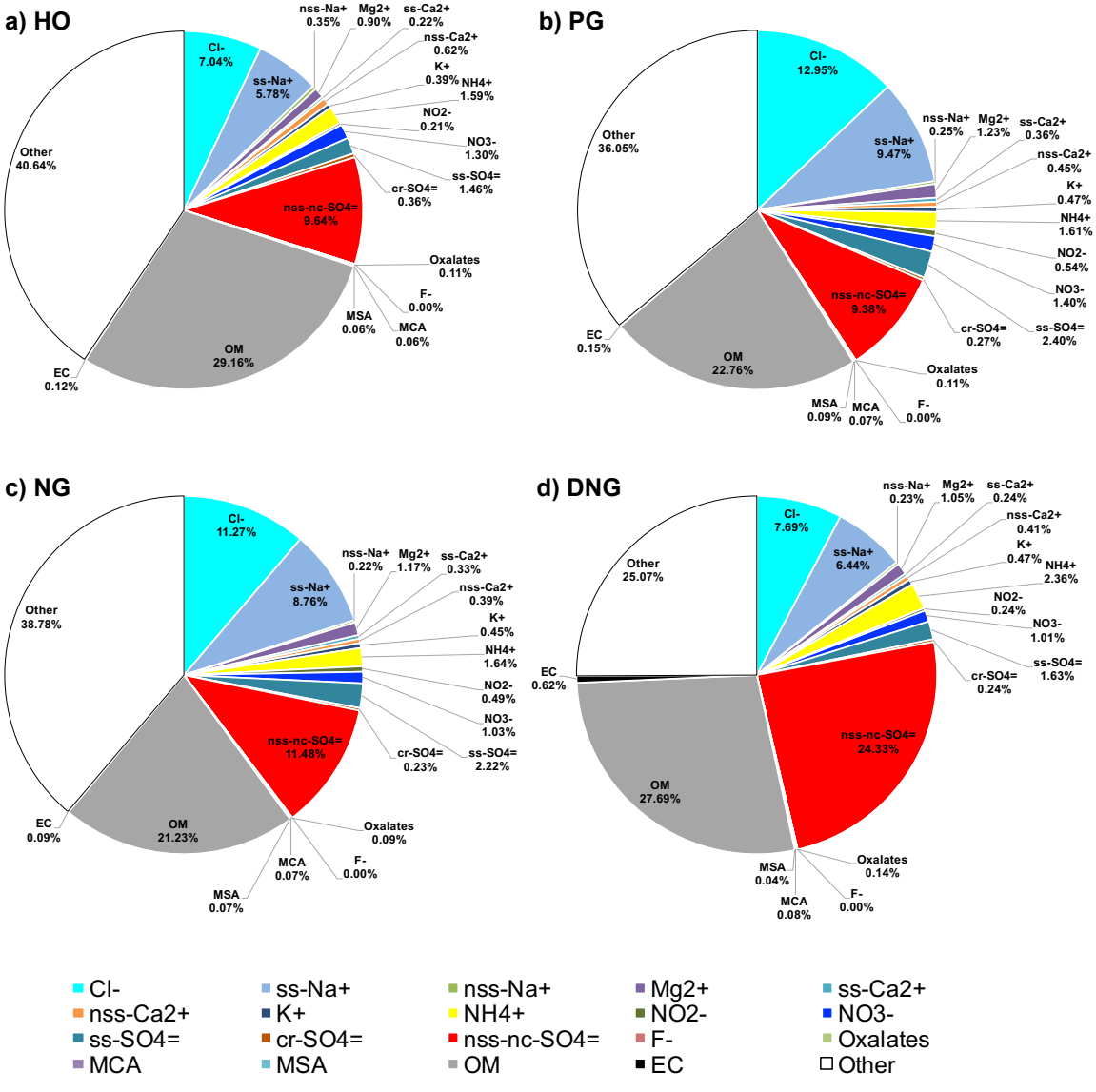

Figure 8. Springtime aerosol chemical composition determined at ground during: a) homogeneous profiles (HO); b) positive gradient profiles (PG); c) negative gradient profiles (NG); d) decoupled negative gradient profiles (DNG). Data shown are the respective aerosol mass fractions of each individual aerosol species.

Atmos. Chem. Phys. Discuss., doi:10.5194/acp-2016-171, 2016
Manuscript under review for journal Atmos. Chem. Phys.
Published: 13 April 2016

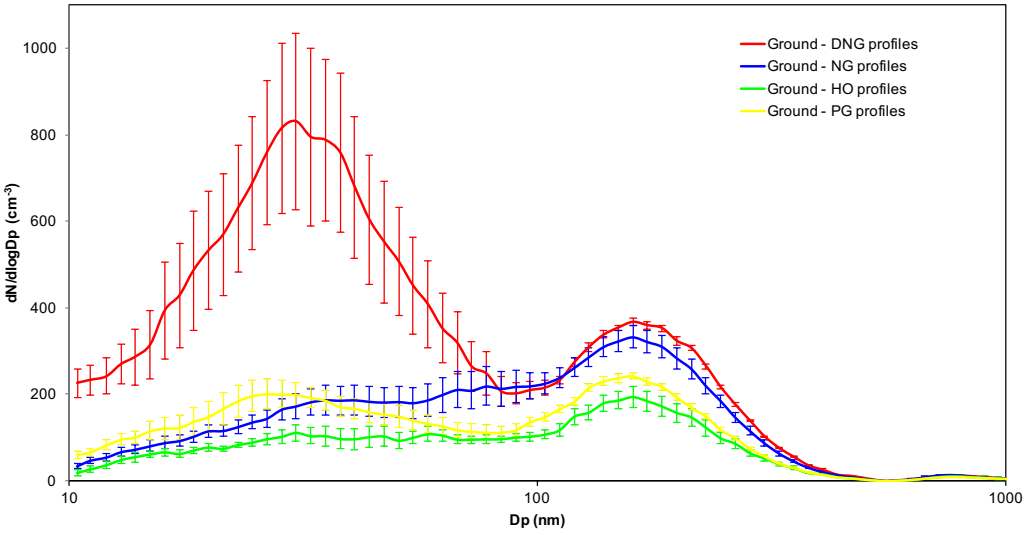

Figure 9. Springtime aerosol number size distribution measured at ground and timely coincident with: homogeneous profiles (HO), positive gradient profiles (PG), negative gradient profiles (NG) and decoupled negative gradient profiles (DNG).

Atmos. Chem. Phys. Discuss., doi:10.5194/acp-2016-171, 2016
Manuscript under review for journal Atmos. Chem. Phys.
Published: 13 April 2016

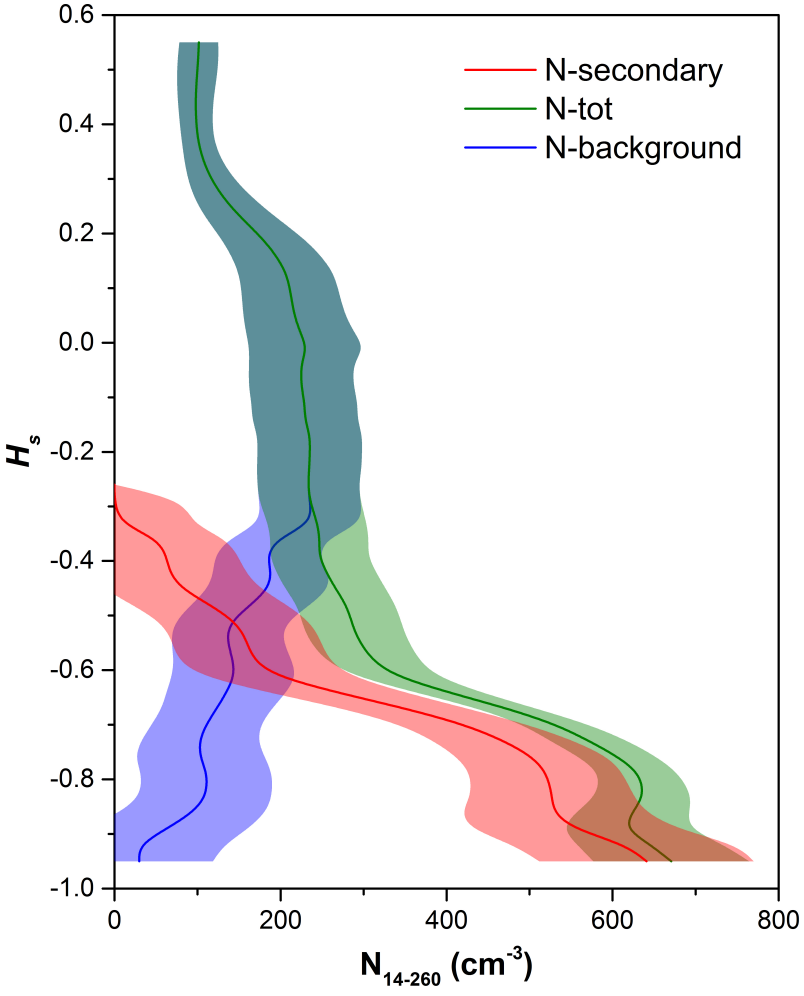

Figure 10. Springtime statistical mean profiles of $N_{14\text{-}260}$ (green line) apportioned along height for the contribution of background $N_{14\text{-}260}$ aerosol (blue line) and secondary locally formed $N_{14\text{-}260}$ aerosol (red line) for the decoupled negative gradient profiles (DNG) category.

Atmos. Chem. Phys. Discuss., doi:10.5194/acp-2016-171, 2016
Manuscript under review for journal Atmos. Chem. Phys.
Published: 13 April 2016

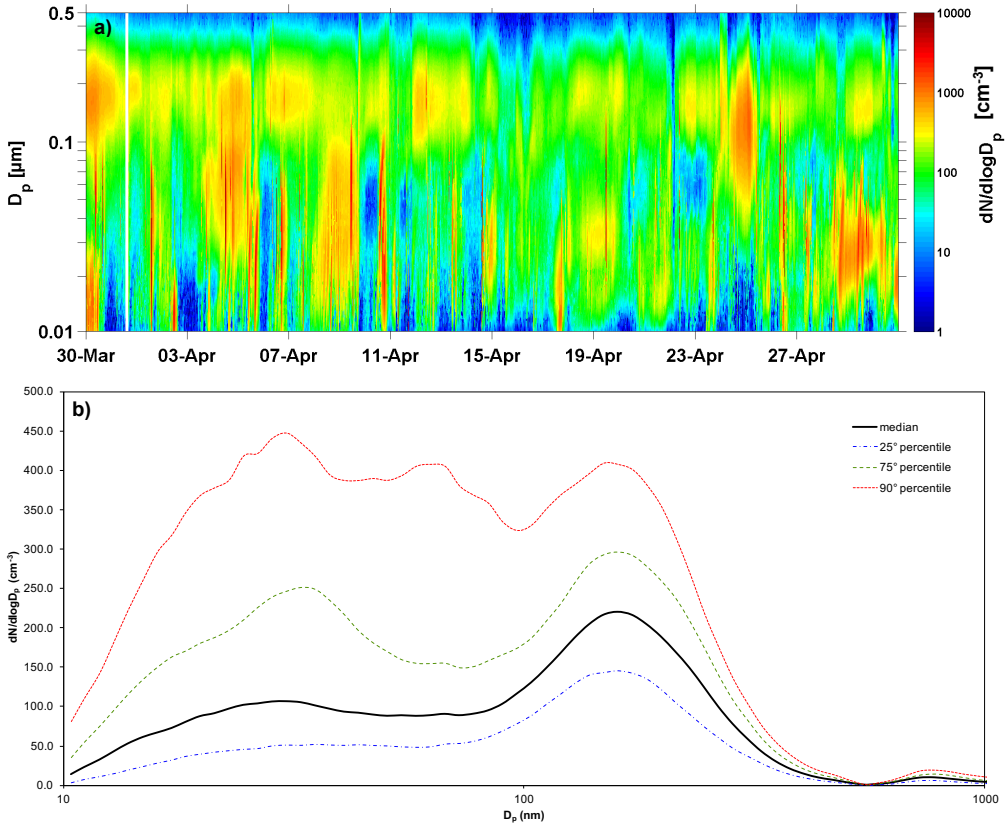

Figure 11. a) aerosol number size distribution measured at ground during April 2011; b) 25°, 50°, 75° and 90° percentiles of the measured number size distribution.

Atmos. Chem. Phys. Discuss., doi:10.5194/acp-2016-171, 2016
Manuscript under review for journal Atmos. Chem. Phys.
Published: 13 April 2016

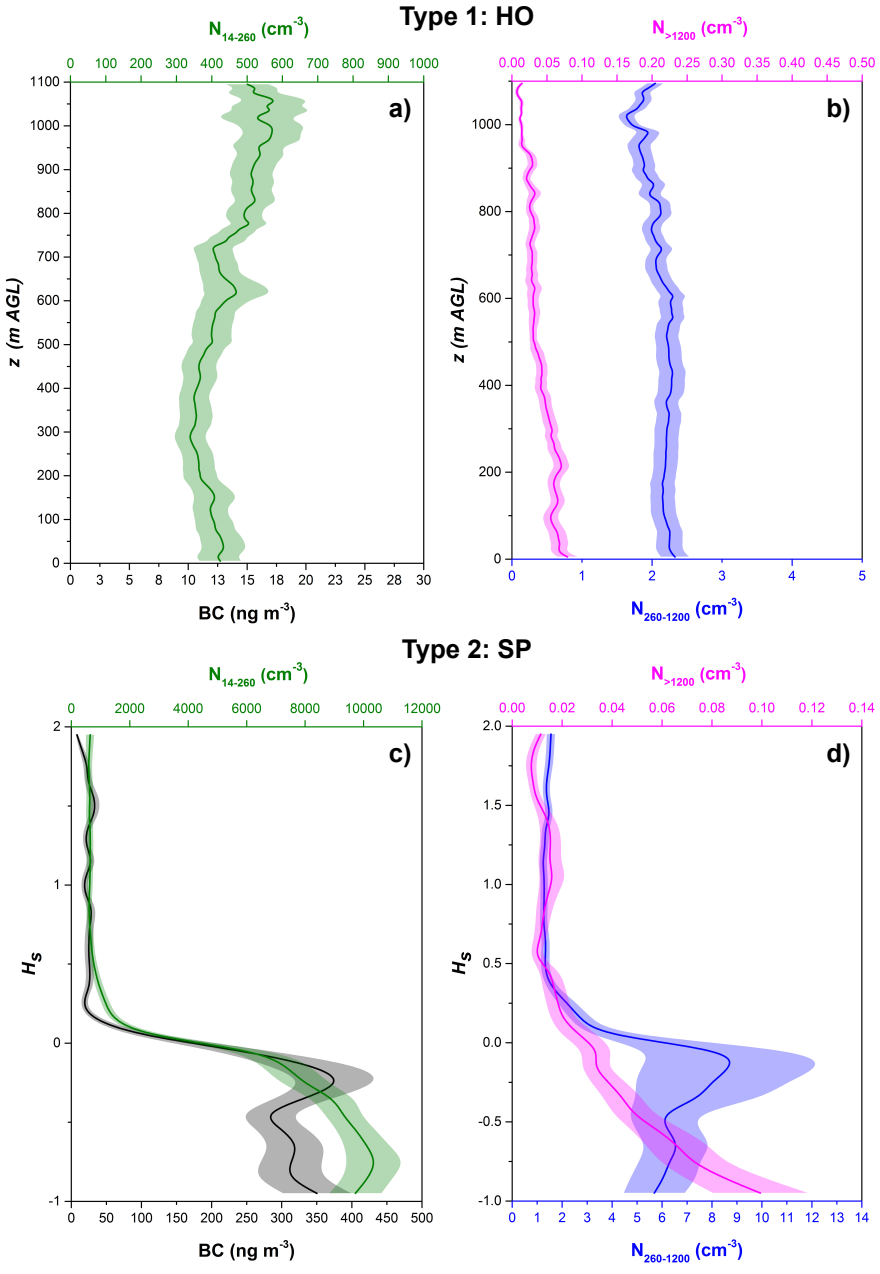

Figure 12. Summertime statistical mean profiles of $N_{14\text{-}260}$ (green line), BC (black line), $N_{260\text{-}1200}$ (blue line) and $N_{>1200}$ (magenta line) along standardized height H_s over Ny-Ålesund for the two typologies of vertical profiles: a-b) homogeneous profiles (HO); c-d) profiles impacted by shipping emissions (SP).

Atmos. Chem. Phys. Discuss., doi:10.5194/acp-2016-171, 2016
Manuscript under review for journal Atmos. Chem. Phys.
Published: 13 April 2016

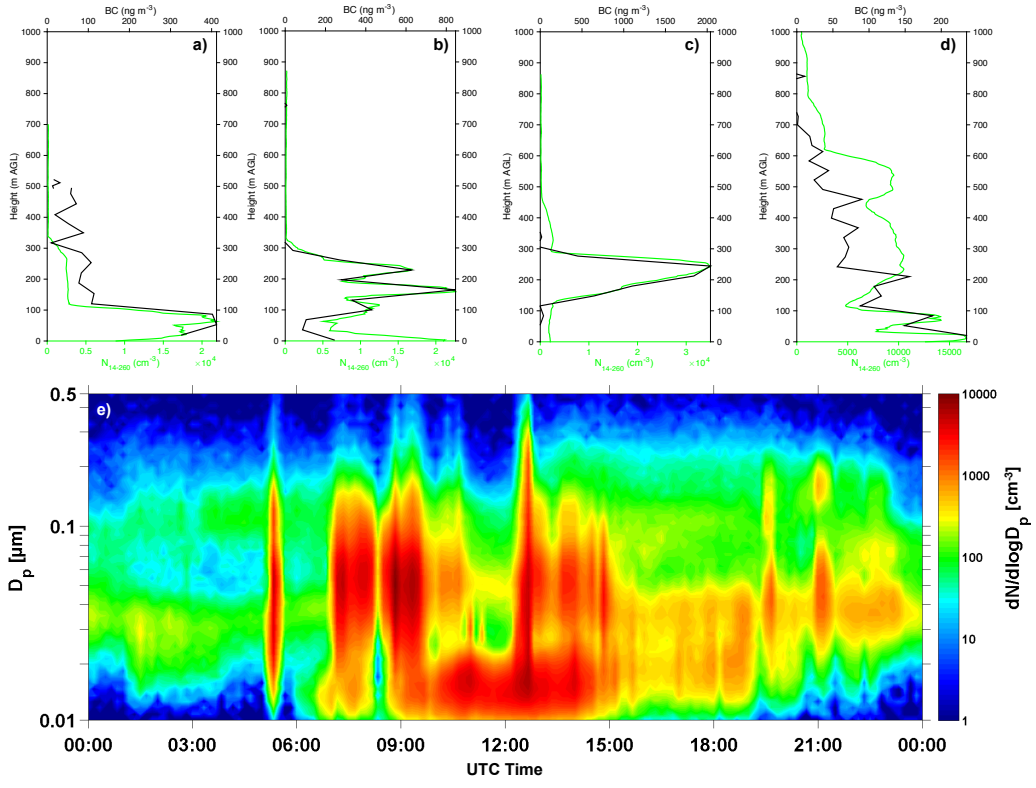

Figure 13. Case study of 6th July 2011 when four ships anchored (not simultaneously) in the harbor of Ny-Ålesund. Vertical profiles of $N_{14\text{-}260}$ (green line) and BC (black line) (0740 UTC, 0901 UTC, 0932 UTC and 1340 UTC) are reported in panels from a) to d) together with ground SMPS data collected at Gruvebadet (e). Note the change in BC scale to progressively increasing BC values during the peak of the ship activity at mid-day.